Faculty of Engineering

University of Southern Denmark

Automated modal analysis of an airfoil

Profiling project

Author:

Casper Aaskov Drangsfeldt

Supervisor:

Ass. Prof. Luis David Avendaño-Valencia

Version Number
May 31, 2022

Preface

This profiling project supports the main work in the master thesis. The master thesis is part of the master's degree Structural Engineering at the University of Southern Denmark. The profiling project is written by Casper Aaskov Drangsfeldt with the supervision from Luis David Avendanõ-valencia.

Casper Aaskov Drangsfeldt

Casper Drangsfeldt

Signature

31-05-2022

Date

Abstract

Nowadays with the urge to obtain renewable energy, the pursuit for larger wind turbines is growing rapidly. Simultaneously, the locations are becoming more remote. As a consequence the complications bound to maintenance are building up. In short, the need for a *Structural Health Monitoring* (SHM) system is increasing. For the SHM system to detect a damage as early as possible it is necessary to reduce the uncertainty bounds of the *Damage Sensitivity Features* (DSF). Several system identification methods, both non-parametric and parametric, for extraction of the *Modal Parameters* (MP) of a *Finite Element* (FE) representation of a laboratory-scaled wind turbine blade are analyzed in terms of the associated bias and the variance. The bias and the variance of each system identification method are estimated using extensive Monte Carlo simulations. The result hereof showed that the *Output Only* (OO) based *AutoRegressive* models had high accuracy in terms of less bias and variance. Similar accuracy was seen for MP extraction with the use of the *Power Spectral Density* (PSD) obtained from the outputs.

Contents

List of Figures

Introduction

One of the challenging tasks today regarding global warming and the emission of vast amounts of CO_2 is to obtain renewable energy. A renewable energy source is wind energy, and mankind has harvested this type of energy for decades.While attempting to harvest more energy from the wind, the size of wind turbines is growing rapidly and the location has been more remote. New challenges arises when moving to a remote location, namely maintenance and service. The cost of transporting crew and equipment to a remote location can be a significant matter. To minimize these expenses, the maintenance and services must be tightly scheduled, based on previous experience. [Mei]. While limited knowledge of how bigger turbines perform compared to existing turbines, these schedules will not guarantee unexpected breakdowns. Therefore, the risk of unexpected breakdowns can be minimised by implementing a *Structural Health Monitoring* (SHM) system.

In the initiation phase of developing a vibration-based SHM system an essential step is the estimation and selection of features related to the structure which are sensitive to damage. The sensitivity of the feature determines how early damage can be detected. An example of such features can be the *Modal Parameters* (MP) of the structure. In the context of damage detection, it can be difficult to distinguish if a change in the MP is due to damage or the *Environmental and Operational Variability* (EOV). Furthermore, deviations in the estimated MP are unavoidable independent of the method used for estimation [Per+20]. For estimation of the MP several different methods exist. For modal analysis, the consistency and thereby the deviation of the MP estimate is of importance due to the inevitable randomness in signals. Therefore, the main focus of this study is to compare the stability and uncertainty bounds of the MP estimates obtained with different *Operational Modal Analysis* (OMA) and *Experimental Modal Analysis* (EMA) methods in the context of SHM. To quantify the uncertainties introduced by the different methods, a *Finite Element* (FE) model of a laboratory-scaled wind turbine blade has been built.

State of the art

Several methodologies for MP estimates are present in the research field today. One technique based on the *Power Spectral Density* (PSD) of the output is stated in [PP22]. For this study, a vibration-based damage detection technique of a wind turbine blade with the use of OMA is proposed. The MPs of the modelled structure are extracted using the *Frequency Domain Decomposition* (FDD) of the PSD of the output based on 11 measured responses. The *Mode Shape Difference* (MSD) is then used as *Damage Sensitive Feature* (DSF) to detect and localize the applied damages. Even though it was possible to detect and localize the damages introduced, the uncertainties of the extracted MP are not estimated, which may have an effect on the minimum amount of damage that can be detected by the algorithm. Furthermore, proper localization of the damage using the MSD method requires certain amounts of measured responses.

Another technique based on a parametric representation of the signal used for estimating the natural frequency of a wind turbine blade is suggested in [Cha+21]. The methodology in this paper is based on the statement that the blades on a healthy wind turbine behave identically and that the three blades are exposed to the same EOV. *Gaussian Process* (GP) is trained to estimate the natural frequency of one blade given the frequency of another healthy blade. The training process occurs in the first two years of the lifetime of the wind turbine to avoid damages in the training phase. After the two year training period, the residual errors of the GP's for a six month period were calculated and used as a threshold. If the estimated edge frequency of one of the blades exceeds this threshold, it is assumed that damage is present. The proposed SHM may not be able to detect if the same sort of damage occurs for the blades simultaneously, but this event may be extremely rare. Furthermore, if a manufacturing fault is present in one of the blades, this method might be slightly inaccurate.

The use of the Gaussian Process for system identification of a signal is further developed in [AC19]. Two methods for system identification are proposed for *Linear Parameter Varying* (LPV) systems, local and global identification. The first method is based on local models which then are interpolated using GP regression. The second method is the *Expectation-Maximization* (EM) algorithm used on the entire training set. To reduce the computational load a parametric form of the GP's with the use of a time-series model, AutoRegressive, is used (GP-AR). The obtained data originate from a FE representation of a wind turbine blade. For the representation of the excitation, aerodynamic loads were calculated. For the LPV varying temperatures and wind speed based on measured data for a whole year are included in the model. The objective is to assess the performance of the proposed methods and not the attainment of the MP estimates. It was concluded that the advantage of the global identification method was the accuracy of the estimated dynamics. Furthermore, using the parametric form of the GP's with time-series model for damage detection is feasible.

Independently on the method used for MP estimation, uncertainties will be inevitable. For the obtainment of high accuracy, the uncertainties can be investigated. The uncertainties of the identified MP using the *Covariance-driven Stochastic Subspace Identification* (SSI-Cov) are estimated in [Per+20]. The subspace identification methods are based on the state-space model of the system which the MP then can be extracted from. The use of SSI-Cov for system identification provides numerous modes, both physical and numerical. With a method based on Hierarchical clustering closely spaced poles, defined by calculating the distance between, are clustered in one mode. To sort the numerical poles within the cluster, mode shapes for each pole are compared with predefined reference mode shapes using the *Modal Assurance Criterion* (MAC). If it is above a certain threshold it is assumed to be a physical mode. The cluster containing physical modes extracted by using SSI-Cov is then used for the prediction of the standard deviation. The methodology can be used for increasing the accuracy of the MP. In the context of SHM knowledge of the standard deviation of the features can improve the process of moving outliers. One possible disadvantage can occur if closely spaced modes of the structural dynamics are present since there will be a risk of a common cluster.

A similar approach is proposed in [RPD08]. With the use of SSI-Cov/ref (reference-based generalization of the covariance-driven stochastic subspace identification method) is used to extract the MP. To sort out numerical and noisy modes, several thresholds for the deviation of the frequencies and damping ratios for each model order are set. Furthermore, the MAC and the modal transfer norm are used to ensure the selection of only physical modes. To minimize the bias of the estimated MP the stabilization diagram is analysed where a suitable model order is selected. Afterwards, the uncertainty bounds related to the MP are estimated from the covariances between the MP. This allows estimation of the uncertainty bounds from only a single data set. To validate the estimated bounds Monte-Carlo simulations have been conducted as a reference. The same problem as mentioned in the previous method can occur. If closely spaced modes are present a complex model structure of the SSI-Cov/ref to separate the modes might be unavoidable. A complex model structure can lead to significant amounts of spurious modes, which may conflict with the physical modes.

Another method for estimating the uncertainties bound with MP estimation is proposed in [Gre+22]. Whereas the previous estimation of the uncertainties originates from the covariance-driven stochastic subspace identification, both data-driven and covariance-driven SSI for both *Input-Output* (IO) and *Output-Only* (OO) are analysed. The statistical Delta method is then used to estimate the uncertainties bound with the estimated MP using only one data set. The statistical Delta method is then validated concerning the distribution of the MP estimates obtained from Monte Carlo experiments. A general agreement between the variance of the estimated MP from the statistical Delta method and the Monte-Carlo simulations is seen. But for some of the modes, a consensus between the two methods is not present. Therefore, for a thorough validation of the estimated MP obtained from a selected system identification method the use of Monte-Carlo simulations is expected to be the most accurate.

Methodology

Throughout the investigation of state-of-the-art on prediction of the uncertainty bounds associated with MP estimation, the Monte-Carlo simulations are typically used for validating of different techniques. Since the aim of the study is the accuracy of different MP extraction techniques, and not how to easily obtain the uncertainty bounds, the Monte-Carlo simulations will be used for this purpose.

The overall methodology can be viewed in the following flow chart:

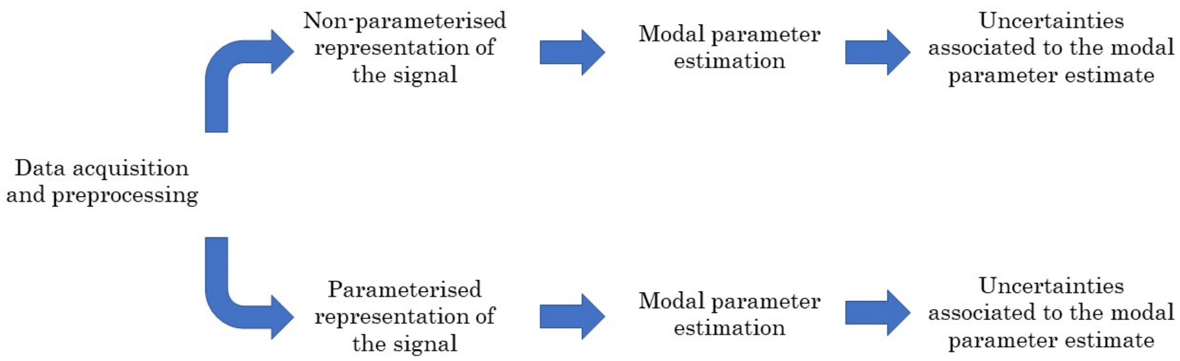

Figure 1.1: Flow chart of the processes throughout this study

- **Data acquisition and preprocessing** involves the process of acquire the vibration-based data of the given structure. A theoretical structure (FE representation of a given structure) has been built so that the estimated MP can be compared to the actual values.
- **Representation of the vibration-based signal** is then performed using different techniques, both non-parametric and parametric methods. The methods are analyzed in order to enhance the performance.
- **Modal parameter estimation** from the different techniques is then carried out.
- **Uncertainties associated to the modal parameter estimate** are analysed by the use of Monte-Carlo simulations.

1.1 Data acquisition and preprocessing

As basis for comparison of the performance of the different parametric methods, a FE model is build using Euler-Bernoulli elements. This FE model is a coarse representation of a laboratory scaled wind turbine blade fixed at the root of the blade [GF16]. Since the natural frequencies and damping ratios of the FE model are known, the bias of the estimated MP can be determined.

1.1.1 The FE model

The parameters of the FE model is as follows (see Table 1.1). The cross-sectional area, which constitute a rectangle, changes for each element within the model, but the length of the elements are constant. Furthermore, the material properties for fiberglass reinforced epoxy, which are typically used for wind turbine blades, are dependent of the direction of the fibers. For this FE model, only flapwise vibrations are analysed. Therefore, the longitudinal modulus of elasticity is used. [Has15].

System Parameters of the FE model	
Modulus of Elasticity	$40GPa$
Density	$1900\frac{kg}{m^3}$
Length	$0.71m$
Dimension at root	$0.07\times0.02m^2$
Dimension at tip	$0.03\times0.02m^2$
Maximum dimension	$0.135\times0.045m^2$
Boundary Conditions	Fixed-Free
Number of elements	50

Table 1.1: System parameters of the FE model.

The changing height and width of the model is illustrated in Figure 1.2. The figure illustrate the constant cross-sectional area for each element and the variation of cross-sectional area between the elements.

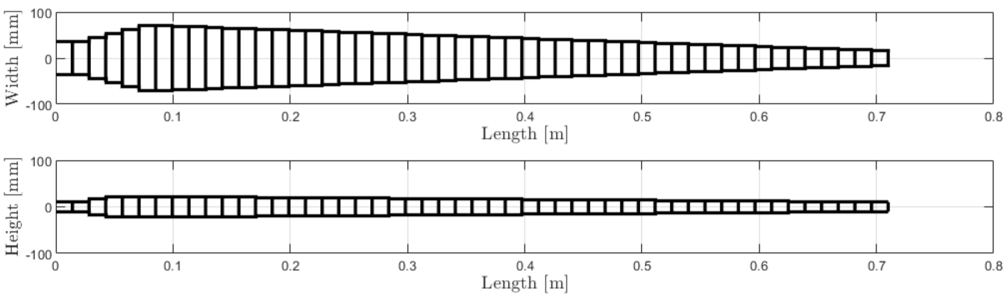

Figure 1.2: Height and width of the FE model

With the given parameters, it leads to the equation of motion of the FE model:

$$[M]\{\ddot{x}\} + [K]\{x\} + [C]\{\dot{x}\} = \{F\} \tag{1.1}$$

where the mass matrix of the Euler-Bernoulli beam is calculated for each element as:

$$\boldsymbol{m} = \frac{\rho AL}{420}\begin{bmatrix} 156 & 22L & 54 & -13L \\ 22L & 4L^2 & 13L & -3L^2 \\ 54 & 13L & 156 & -22L \\ -13l & -3L^2 & -22L & 4L^2 \end{bmatrix} \tag{1.2}$$

and the stiffness of each element is calculated as:

$$\boldsymbol{k} = \frac{EI}{L^3}\begin{bmatrix} 12 & 6L & -12 & 6L \\ 6L & 4L^2 & -6L & 2L^2 \\ -12 & -6L & 12 & -6L \\ 6L & 2L^2 & -6L & 4L^2 \end{bmatrix} \tag{1.3}$$

The damping of the FE model is modelled as modal damping where a damping factor is added to each undamped natural frequency to then calculate the poles of the system. [Bra11]. For this FE structure, different damping factors for the first our modes have been added:

$$\boldsymbol{\zeta} = \begin{Bmatrix} 0.005 \\ 0.01 \\ 0.015 \\ 0.02 \end{Bmatrix} \tag{1.4}$$

The excitation is modelled as a excitation acting in a single node to simulate the same setup as in [GF16]. A thorough description of the excitation is present in Section 1.1.2.

1.1.2 Setup of the FE model

Since all the parameters of the FE model are known, an analytical modal analysis can be performed to obtain the natural frequencies and mode shapes. The mode shapes are then plotted to estimate a proper location to simulate the response. Four locations to simulate the response and one location for the excitation are chosen and shown with the first four modes in Figure 1.3.

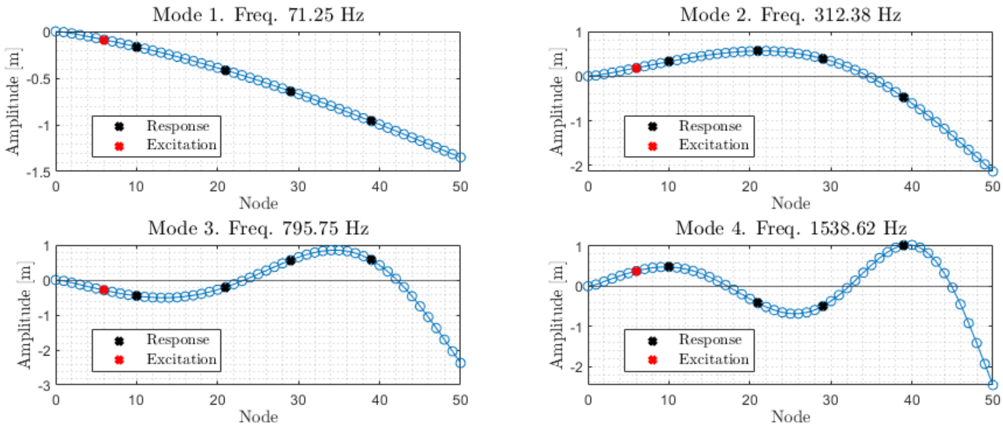

Figure 1.3: The first four analytical modeshapes, with the chosen excitation and response locations. Also, the natural frequency for each mode are shown above the plot of the modeshape. The modeshapes are normalized for unit modal mass.

In preparation for OMA, where it is essential to model the input as white Gaussian noise [BE15b], the excitation of the FE model is modelled as pure white Gaussian noise with a variance of 10. The effect of white Gaussian noise in the input is seen in the auto-correlation. In the auto-correlation of the input at a time-lag of 0 the peak correspond to the variance. Furthermore, no correlation is seen at any other time lag indices. The auto-correlation of the input is seen in Figure 1.4.

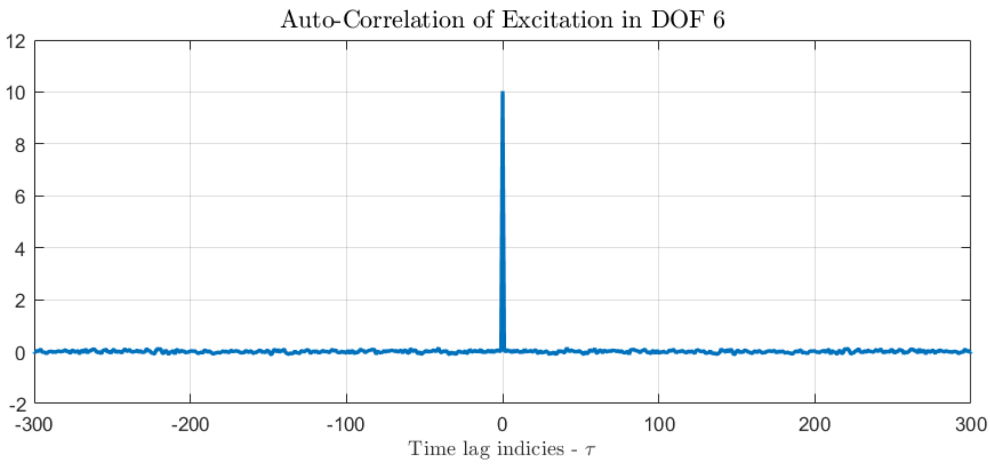

Figure 1.4: Auto-correlation of the input. At time lag 0, the auto-correlation equals the variance.

Lastly, to ensure a stable MP estimation using parametric methods for the simulated time responses, white Gaussian noise have also been added to the output signal. This added noise should represent any unwanted random noise through the data acquisition process. Therefore, the variance of the noise added to the output should be far less significant than the pure white Gaussian noise in the input. The variance for the output noise is set to $1 \cdot 10^{-5}\%$ of the variance of the input. The auto-correlation of the each responses is seen in Figure 1.5.

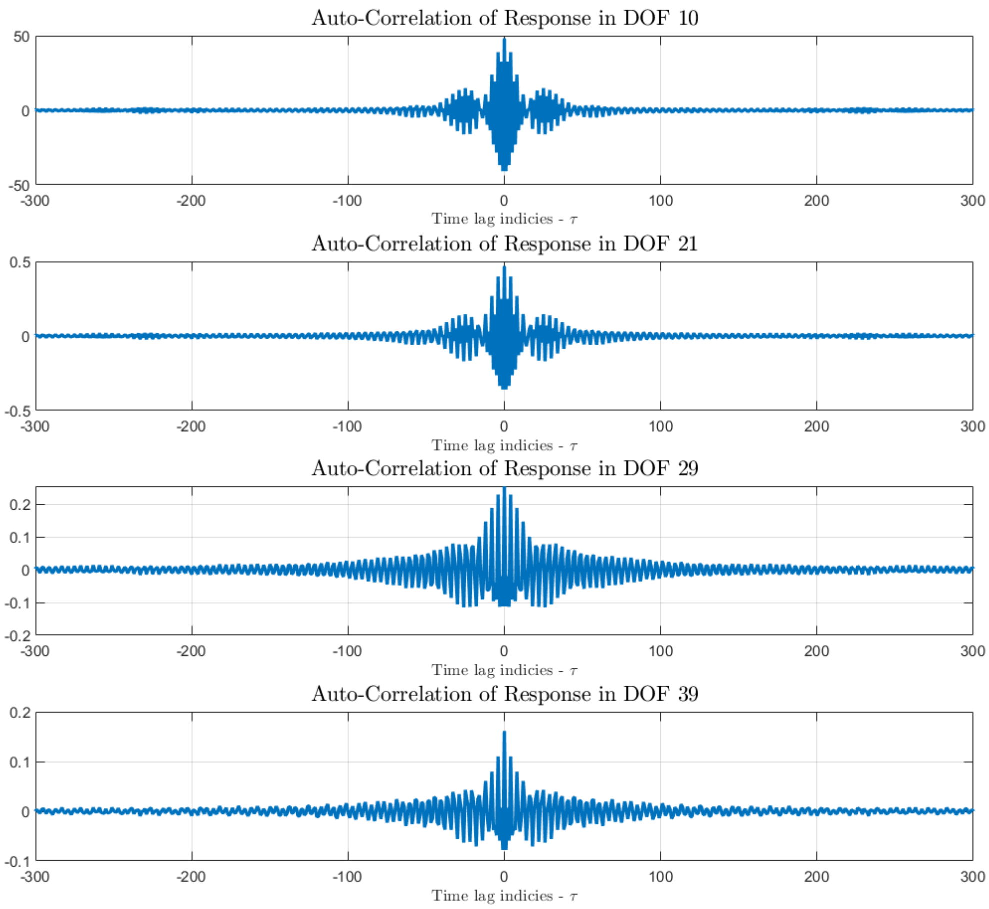

Figure 1.5: Auto-correlation of the output where the auto-correlation for each response is illustrated.

With the described system setup, it is crucial to check the multiple coherence, since white Gaussian noise is present in both input and output. The check of the coherence provides an overview of how close the estimated *Frequency Response Function* (FRF) is to the true FRF. If unity is reached then the estimate is equal to the true FRF.

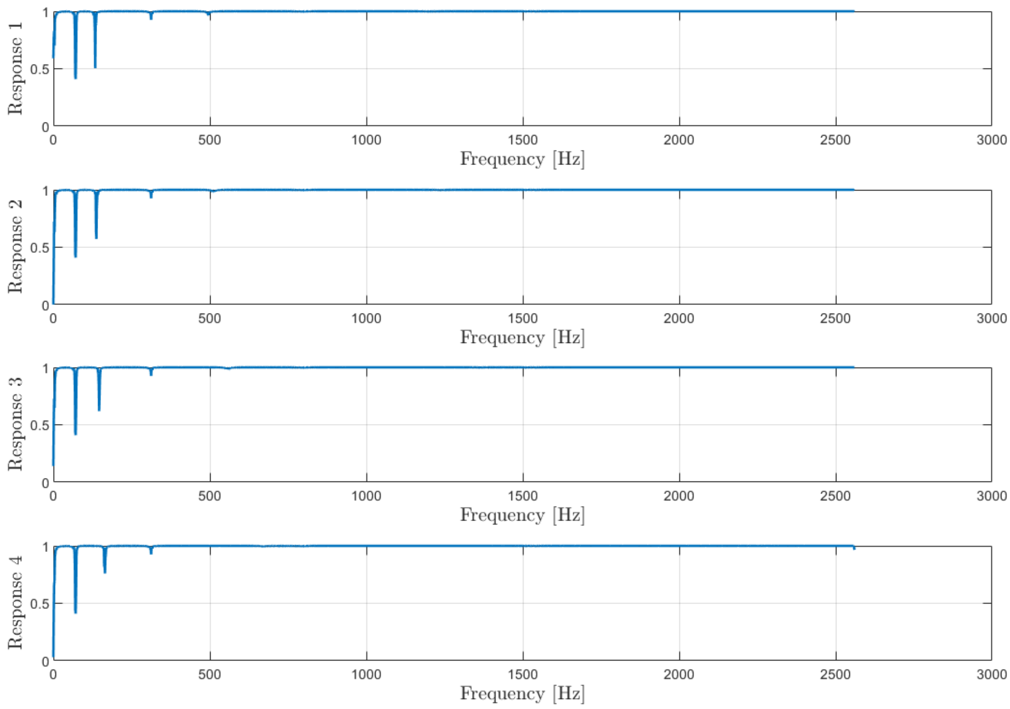

Figure 1.6: Multiple coherence calculated from PSD obtained using Welch's estimator, see Section 1.2.1, with a blocksize equal to one quarter of the total blocksize, overlap of 75% and with the use of Hanning window.

The multiple coherence is shown in Figure 1.6. Significant drops are seen at the first and second natural frequencies. Although it is wanted to have a coherence near unity, drops will typically appears at the natural frequencies. These drops can be reduced if the noise are reduced, but this is not possible to reduce entirely in real-life setups. [Bra11].

1.2 Representation of the vibration-based signal

Two main methods for representation of a measured signal are available, namely non-parametric and parametric methods. Both methods have different advantages and disadvantages. The best method mostly depends on the user's experience and stance. [Bra11] [Ave] [BV15].

1.2.1 Non-parametric methods

In most vibration analysis it is typically wanted to analyse the frequency content in the measured signal. If the measured signal is pure periodic, the frequency content consist of discrete frequency lines since the signal only consist of waves with a specific frequency. In reality it is complicated to obtain a pure periodic signal, since the signal usually will be contaminated with some noise as well.

Some signals can have a random behaviour with respect to time, and these signals are called random signals, comprising noise. It is common for all random signals that they contain all frequencies, which are seen as continuous in the frequency spectra and not as discrete frequency lines as for a pure periodic signal. Therefore, one method of analysing the frequency content is by calculating the PSD. [Bra11]. The PSD can be defined as the Fourier transform of the correlation function, [BE15a]

$$G_y = \frac{1}{2\pi}\int_{-\infty}^{\infty} R_y(\tau)e^{-i\omega t}\,d\tau \tag{1.5}$$

Where the correlation function is calculated as the expected value between the response at a time instance and the response at the same time instance plus a time lag, τ, [BE15b]:

$$R_y = E[y(t)y(t+\tau)] \tag{1.6}$$

The PSD is a non-parametric method and it does not requires specific information about the signal. Therefore, it is a rather simple method to used for obtaining an estimate of the MP. A typically PSD calculated as in (1.5) is seen in Figure 1.7.

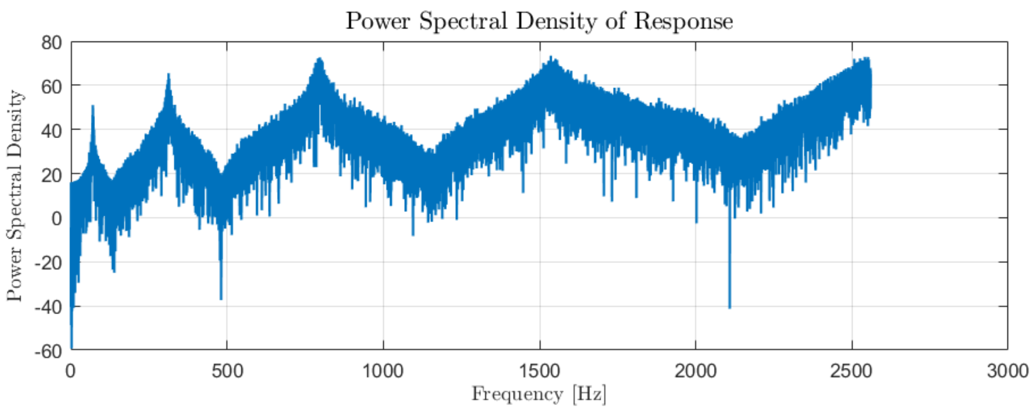

Figure 1.7: Typically PSD calculated as the Fourier Transform of the auto-correlation of an output.

It is seen that there is several distinguish areas where the power is more significant. These peaks represent the damped natural frequency, since the power is increased at resonance. The damped natural frequency for low damped system is near equal to the natural frequency. Furthermore, by using a 3dB bandwidth on each resonance peak, the relative damping factor can be determined as, [Bra11]:

$$\zeta \approx \frac{B_r}{2f_d} \tag{1.7}$$

Where:

$B_r =$ 3dB bandwidth
$f_d =$ Damped natural frequency

One of the disadvantages of using non-parametric methods for estimating the MP is the accuracy. A significant amount of noise can be seen in the PSD in Figure 1.7. This can lead to a less accurate estimate of the MP, especially when estimating the relative damping factor. To increase the accuracy, several different methods exist. Also, it is possible to tune each method to obtain better MP estimates.

1.2.1.1 Obtaining the best PSD estimate

Calculating the PSD from Equation (1.5) were commonly used before the *Fast Fourier Transform* (FFT) algorithm was invented, due to the lack of computational power. Therefore, the correlation function was calculated as in Equation (1.6). Afterwards, with the use of the Wiener-Khinchine relations, the PSD estimate was obtained. This is also known as the Blackman-Tukey method. But after the FFT algorithm were invented, more efficient method were introduced. One of these published methods were the Welch's estimator, which is still commonly used today. [Bra11].

The Welch's estimator is based on the Periodogram. The Periodogram is the squared magnitude of the *Discrete Fourier Transform* (DFT) of the entire signal:

$$\hat{P}_{yy}(k) = \frac{1}{L}\left|\sum_{n=0}^{L} y(n)e^{\frac{-j2\pi kn}{N}}\right|^2 \tag{1.8}$$

Where:

$$\begin{aligned} L &= \text{Length of signal} \\ N &= \text{Blocksize} \end{aligned}$$

For the Welch's estimator instead of taking the DFT of the entire signal, the signal is divided into segments. Each section is then windowed to reduce the effect of leakage. Then the DFT is calculated and all the sections are then averaged to reduce the random error. Also, the sections can have some overlapping to reduce the random error even more. The PSD estimate obtained by the Welch's estimator is:

$$\hat{G}^{W}_{yy}(k) = \frac{S_P}{M}\sum_{m=1}^{M}\left|Y_{w,m}(k)\right|^2 \tag{1.9}$$

Where:

$$\begin{aligned} S_P &= \text{Scaling factor} \\ M &= \text{Number of segments} \\ Y_{w,m} &= DFT[y(n)\cdot w(n)] \\ w(n) &= \text{Spectral window on } n\text{-samples} \end{aligned}$$

The parameters of the Welch's estimator have to be tuned to obtain the best estimates. One of the parameters is the number of segments which the signal is divided into. Too many segments decreases the quality of the frequency resolution, whereas too few segments will not decrease the random error. Also, a suitable spectral window have to be chosen to reduce the the effect of leakage as much as possible. [Bra11].

The same signal as seen in Figure 1.7 is divided into segments with a blocksize $\frac{1}{4}$ of the original blocksize and with an overlap of 75% of the windowed samples. The spectral window used was a Hanning window. The PSD estimate from the Welch's estimator is seen in Figure 1.8. If the PSD estimate is compared with Figure 1.7, it is clear to see that a large amount of the noise have been reduced. Therefore, more accurate MP estimates can be obtained.

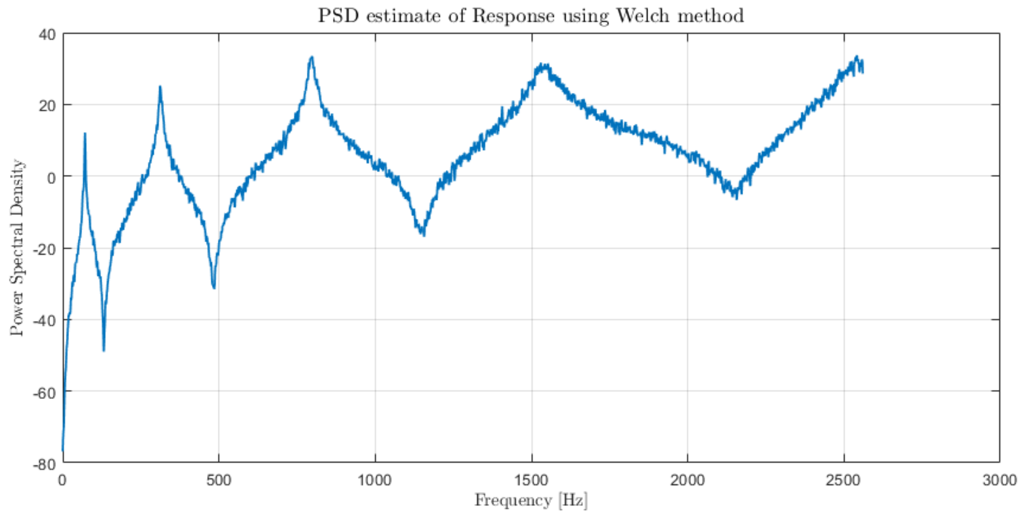

Figure 1.8: PSD estimate using the Welch's method tuned in to produce an acceptable estimate

1.2.2 Parametric methods for extracting modal parameters

In 1.2.1 the MP extraction were from a non-parameterized model of the signal in the frequency domain. This method is relatively simple but the accuracy may be impaired. Another methodology for extracting MP is by using a parameterized representation of the signal. The process initiates with selecting a model structure with some free parameters. These parameters are then adjusted such that the model fits the observed signal. The parametric methods can be inefficient if an unsuitable model structure is selected. To select a suitable model structure, prior information is crucial. This prior information can be provided by a non-parametric visualization of the signal. One crucial error can occur if the system is not *Linear Time Invariant* (LTI), which is one of the main assumption in the listed methods below. Another important assumption before choosing model structure is if the system can be modelled as *Single-Input Single-Output* (SISO) or *Multiple-Input Multiple-Output* (MIMO). [Ave]. To yield an understanding of different parametric methods for system identification, the following methods are shortly enlighted before analyzing the MP extraction and the associated uncertainty bounds.

- VAR - Vector Auto-Regressive Model
- VARX - Vector Auto-Regressive with eXogenous variable model
- VARMA - Vector Auto-Regressive Moving Average Model
- VARMAX - Vector Auto-Regressive Moving Average with eXogenous variable model
- MITD - Modified Ibrahim Time-Domain (For output only and input-output)
- SSI - Stochastic Subspace Identification Algorithm
- ERA - Eigensystem Realization Algorithm (For output only and input-output)

1.2.2.1 Auto-Regressive model (AR-model and VAR-model)

An AR-model is used for a system where only a single output is known. The model structure is based on the observed signal itself $y[n]$, AR-coefficients a_i which are the free parameters of the model, previous observations $y[n-i]$, and some noise which cannot be predicted by previous observations $w[n]$:

$$y[n] = -\sum_{i=1}^{n_a} a_i \cdot y[n-i] + w[n] \tag{1.10}$$

where the noise, $w[n]$, typically named the innovations, is *Normally and Independently Distributed* (NID):

$$w[n] \sim NID(0, \sigma_w^2) \tag{1.11}$$

The characteristic polynomial of the AR-model is obtained as:

$$A(\mathscr{B}) = 1 + \sum_{i=1}^{n_a} a_i \cdot \mathscr{B}^i \tag{1.12}$$

Where:

$\mathscr{B} =$ Backshift operator defined as $\mathscr{B}^i y[n] = y[n-i]$

The roots of the characteristic polynomial yields the natural frequencies,

$$\omega_{n_i} = \mid \log \lambda_i \mid \tag{1.13}$$

and the damping ratios:

$$\zeta_i = -\cos(\arg(\log \lambda_i)) \tag{1.14}$$

If the AR-structure should be used for representation of a MIMO system, a vectorized model structure, VAR, can be used:

$$\boldsymbol{y}[n] = -\sum_{i=1}^{n_a} \boldsymbol{A}_i \cdot \boldsymbol{y}[n-i] + \boldsymbol{w}[n] \tag{1.15}$$

where the innovations now defined as NID with a zero mean and the covariance matrix $\boldsymbol{\Sigma}_w$:

$$\boldsymbol{w}[n] \sim NID(0, \boldsymbol{\Sigma}_w) \tag{1.16}$$

Following the same approach by calculating the roots of the characteristic polynomial, the natural frequencies and damping ratios can be calculated. [Ave]

1.2.2.2 Auto-Regressive Moving Average model (ARMA-model and VARMA-model)

Compared to the AR-model in 1.2.2.1 the ARMA-model consists of one extra term with the MA-coefficients c_i multiplied by the previous innovation, $w[n-i]$ estimated from a long AR-model:

$$y[n] = -\sum_{i=1}^{n_a} a_i \cdot y[n-i] + w[n] + \sum_{i=1}^{n_c} c_i \cdot w[n-i] \tag{1.17}$$

where the innovations of the ARMA-model are NID with zero mean and variance σ_w^2:

$$w[n] \sim NID(0, \sigma_w^2) \tag{1.18}$$

The natural frequencies and damping ratios are determined following the same approach described in 1.2.2.1. Furthermore, the roots of the MA-polynomial predicts the anti-resonances:

$$C(\mathscr{B}) = 1 + \sum_{i=1}^{n_c} c_i \mathscr{B}^i \tag{1.19}$$

Using the ARMA-model for representation of a MIMO-system requires a vectorized structure, namely the VARMA-model:

$$\boldsymbol{y}[n] = -\sum_{i=1}^{n_a} \boldsymbol{A}_i \cdot \boldsymbol{y}[n-i] + \sum_{i=1}^{n_c} \boldsymbol{C}_i \cdot \boldsymbol{w}[n-i] + \boldsymbol{w}[n] \tag{1.20}$$

with the innovations of the VARMA-model being NID with zero mean and covariance matrix $\boldsymbol{\Sigma}_w$:

$$\boldsymbol{w}[n] \sim NID(0, \boldsymbol{\Sigma}_w) \tag{1.21}$$

The natural frequencies and damping ratios can be calculated from the roots of the AR polynomial, Equation (1.13) and (1.14). [Ave]

1.2.2.3 Auto-Regressive with Exogenous variables model (ARX-model and VARX-model)

The models stated in 1.2.2.1 are model structures for when only the output(s) is/are given, this is the OO identification case. By adding Exogenous variables to the model structure, an IO representation of the system is possible, as in the ARX model given by the following expression:

$$y[n] = -\sum_{i=1}^{n_a} a_i \cdot y[n-i] + \sum_{i=1}^{n_b} b_i \cdot x[n-i] + w[n] \tag{1.22}$$

and for MIMO-system, the VARX-model structure is given as:

$$\boldsymbol{y}[n] = -\sum_{i=1}^{n_a} \boldsymbol{A}_i \cdot \boldsymbol{y}[n-i] + \sum_{i=1}^{n_b} \boldsymbol{B}_i \cdot \boldsymbol{x}[n-i] + \boldsymbol{w}[n] \tag{1.23}$$

Again, the natural frequencies and damping ratios can be estimated by finding the roots of the characteristic AR-polynomial, $A(\mathscr{B})$. [Ave].

1.2.2.4 Auto-Regressive Moving Average with Exogenous variables model (ARMAX-model and VARMAX-model)

Similar as in 1.2.2.3, the model structure given in 1.2.2.2 can also be used for IO by adding Exogenous variables to the model structure:

$$y[n] = -\sum_{i=1}^{n_a} a_i \cdot y[n-i] + w[n] + \sum_{i=1}^{n_b} b_i \cdot x[n-i] + \sum_{i=1}^{n_c} c_i \cdot w[n-i] \tag{1.24}$$

Furthermore, for representation for a MIMO-system, a vectorized structure of the ARMAX-model is given as:

$$\boldsymbol{y}[n] = -\sum_{i=1}^{n_a} \boldsymbol{A}_i \cdot \boldsymbol{y}[n-i] + \boldsymbol{w}[n] + \sum_{i=1}^{n_b} \boldsymbol{B}_i \cdot \boldsymbol{x}[n-i] + \sum_{i=1}^{n_c} \boldsymbol{C}_i \cdot \boldsymbol{w}[n-i] \tag{1.25}$$

For both cases, the roots of the AR-polynomial yields the estimate of the natural frequencies and damping ratios. [Ave].

1.2.2.5 Modified Ibrahim Time-Domain (MITD)

Whereas the latter methods for system identification are based on time-series, the MITD is based on free decays extracted from the structure. The formulation of the model is based on a linear combination of the modeshapes and the exponential decays:

$$\boldsymbol{y}(k\Delta t) = \sum_{n=1}^{N} (c_n \boldsymbol{\psi}_n e^{\lambda_n k\Delta t} + c_n^* \boldsymbol{\psi}_n^* e^{\lambda_n^* k\Delta t}) = \sum_{n=1}^{N} (c_n \boldsymbol{\psi}_n \mu^k + c_n^* \boldsymbol{\psi}_n^* (\mu^k)^*) \tag{1.26}$$

Where:

$\boldsymbol{\psi}_n =$ Modeshapes of the n-mode
$c_n\ =$ Modal amplitude at the initial state
$\lambda_n =$ The continuous poles
$\mu\ =$ The discrete poles
$\Delta t =$ Time delay
$k\ =$ The lack of the time delay

The free decays can be calculated in two different approaches according to the system identification scenario (IO or OO). In the OO case, the PSD of the signal is calculated, and by taking the inverse Fourier transform, the free decays (or *Auto-Correlation Function*, ACF) are obtained. In the case of IO the FRF is calculated, and by taking the inverse Fourier transform of the FRF, the free decays (or the impulse response) are obtained. The next step for the MITD is building of the Hankel matrix. For simplicity only 4 blocks are built:

$$\boldsymbol{H} = \begin{bmatrix} \boldsymbol{y}(1) & \boldsymbol{y}(2) & \dots & \boldsymbol{y}(np-3) \\ \boldsymbol{y}(2) & \boldsymbol{y}(3) & \dots & \boldsymbol{y}(np-2) \\ \boldsymbol{y}(3) & \boldsymbol{y}(4) & \dots & \boldsymbol{y}(np-1) \\ \boldsymbol{y}(4) & \boldsymbol{y}(5) & \dots & \boldsymbol{y}(np) \end{bmatrix} = \begin{bmatrix} \boldsymbol{H}_1 \\ \boldsymbol{H}_2 \end{bmatrix} \tag{1.27}$$

then by introducing the Toeplitz matrices for the defined Hankel matrix:

$$\begin{aligned} \boldsymbol{T}_{11} &= \boldsymbol{H}_1\boldsymbol{H}_1^T \\ \boldsymbol{T}_{22} &= \boldsymbol{H}_2\boldsymbol{H}_2^T \\ \boldsymbol{T}_{12} &= \boldsymbol{H}_1\boldsymbol{H}_2^T \\ \boldsymbol{T}_{21} &= \boldsymbol{H}_2\boldsymbol{H}_1^T \end{aligned} \tag{1.28}$$

the system matrices can be estimated as:

$$\begin{aligned} \widehat{\boldsymbol{A}}_1 &= \boldsymbol{T}_{12}\boldsymbol{T}_{11}^{-1} \\ \widehat{\boldsymbol{A}}_2 &= \boldsymbol{T}_{22}\boldsymbol{T}_{21}^{-1} \end{aligned} \tag{1.29}$$

By the use of the eigenvalue decomposition of the estimated system matrices, the MP can be obtained. [BE15c].

1.2.2.6 Stochastic Subspace Identification (SSI)

For the *Stochastic Subspace Identification* (SSI) two overall formulations exist, namely the covariance-driven (SSI-cov) and the data-driven (SSI-data). SSI-cov follows the same methodology as for the MITD-model, except for the building process of the Hankel matrix which instead of being built from the responses, it's built from the covariance of the output [TD14]:

$$\Lambda_i = \frac{1}{N-i}\sum_{k=1}^{N-i} y_{k+i}y_k^T \tag{1.30}$$

$$
\boldsymbol{H}_{p,q} = \begin{bmatrix} \Lambda_0 & \Lambda_1 & \dots & \Lambda_{q-1} \\ \Lambda_1 & \Lambda_2 & \dots & \Lambda_q \\ \vdots & \vdots & \dots & \vdots \\ \Lambda_{p-1} & \Lambda_p & \dots & \Lambda_{p+q-2} \end{bmatrix} \tag{1.31}
$$

For the SSI-data methods, the first step is the building of the Hankel matrix from the responses:

$$
\boldsymbol{H} = \begin{bmatrix} \boldsymbol{y}(1) & \boldsymbol{y}(2) & \dots & \boldsymbol{y}(np-2s+1) \\ \boldsymbol{y}(2) & \boldsymbol{y}(3) & \dots & \boldsymbol{y}(np-2s+2) \\ \vdots & \vdots & \dots & \vdots \\ \boldsymbol{y}(s) & \boldsymbol{y}(s+1) & \dots & \boldsymbol{y}(np-s) \\ \boldsymbol{y}(s+1) & \boldsymbol{y}(s+2) & \dots & \boldsymbol{y}(np-s+1) \\ \boldsymbol{y}(s+2) & \boldsymbol{y}(s+3) & \dots & \boldsymbol{y}(np-s+2) \\ \vdots & \vdots & \dots & \vdots \\ \boldsymbol{y}(2s) & \boldsymbol{y}(2s+1) & \dots & \boldsymbol{y}(np) \end{bmatrix} = \begin{bmatrix} \boldsymbol{H}_1 \\ \boldsymbol{H}_2 \end{bmatrix} \tag{1.32}
$$

where $\boldsymbol{H}_1$ is noted as the past and $\boldsymbol{H}_2$ is noted as the future. The next step is the calculation of the projection matrix of the free decays. The calculation requires the observability matrix:

$$
\boldsymbol{\Gamma} = \begin{bmatrix} \boldsymbol{P} \\ \boldsymbol{PD} \\ \boldsymbol{PD}^2 \\ \vdots \\ \boldsymbol{PD}^{s-1} \end{bmatrix} \tag{1.33}
$$

Where:

$\boldsymbol{P} =$ Observation matrix
$\boldsymbol{D} =$ Discrete time system matrix $exp(\boldsymbol{A}\Delta t)$

Then the projection matrix can be calculated as:

$$
\boldsymbol{O} = \boldsymbol{\Gamma X} \tag{1.34}
$$

Where:

$\boldsymbol{X} =$ Kalman states matrix (Initial conditions for the free decays)

Taking the *Singular Value Decomposition* (SVD) of the projection matrix of the free decays, estimates of $\boldsymbol{\Gamma}$ and $\boldsymbol{X}$ can be calculated:

$$
\begin{aligned} \widehat{\boldsymbol{\Gamma}} &= \boldsymbol{U}_n\sqrt{\boldsymbol{S}_n} \\ \widehat{\boldsymbol{X}} &= \sqrt{\boldsymbol{S}_n}\boldsymbol{V}_n^T \end{aligned} \tag{1.35}
$$

which is used for the calculation of $\boldsymbol{D}$ and $\boldsymbol{P}$, from where the MP can be found. [BE15c].

1.2.2.7 Eigensystem Realization Algorithm (ERA)

The overall idea of ERA is the representation of the state-space model and the modelling of free decays. First, the free decay matrix is formulated as:

$$\boldsymbol{Y}(k) = \begin{bmatrix} \boldsymbol{y}_1(k), & \boldsymbol{y}_2(k), & \dots \end{bmatrix} \tag{1.36}$$

and the initial conditions of the free decays:

$$\boldsymbol{U}_0 = \begin{bmatrix} \boldsymbol{u}_{01}, & \boldsymbol{u}_{02}, & \dots \end{bmatrix} \tag{1.37}$$

Then the free decays with the initial conditions can be formulated as:

$$\boldsymbol{Y}(k) = \boldsymbol{P}\boldsymbol{D}^k\boldsymbol{U}_0 \tag{1.38}$$

From this common formulation of the free decays, the two Hankel blocks can be written as:

$$\boldsymbol{H}(0) = \begin{bmatrix} \boldsymbol{Y}(0) & \boldsymbol{Y}(1) & \dots \\ \boldsymbol{Y}(1) & \boldsymbol{Y}(2) & \dots \\ \vdots & \vdots & \dots \\ \boldsymbol{Y}(s-1) & \boldsymbol{Y}(s) & \dots \end{bmatrix} = \boldsymbol{\Gamma\Lambda} \tag{1.39}$$

$$\boldsymbol{H}(1) = \begin{bmatrix} \boldsymbol{Y}(1) & \boldsymbol{Y}(2) & \dots \\ \boldsymbol{Y}(2) & \boldsymbol{Y}(3) & \dots \\ \vdots & \vdots & \dots \\ \boldsymbol{Y}(s) & \boldsymbol{Y}(s+1) & \dots \end{bmatrix} = \boldsymbol{\Gamma D\Lambda} \tag{1.40}$$

Where:

$$\boldsymbol{\Lambda} = \text{Controllability matrix } \begin{bmatrix} \boldsymbol{U}_0 & \boldsymbol{D}\boldsymbol{U}_0 & \boldsymbol{D}^2\boldsymbol{U}_0 & \dots \end{bmatrix}$$

Taking the SVD of the Hankel matrix in Equation (1.40):

$$\boldsymbol{H}(0) = \boldsymbol{U}\cdot\boldsymbol{S}\cdot\boldsymbol{V}^{\boldsymbol{T}} \tag{1.41}$$

following estimations of the observability and controlability matrices can be made:

$$\begin{aligned} \widehat{\boldsymbol{\Gamma}} &= \boldsymbol{U}\sqrt{\boldsymbol{S}} \\ \widehat{\boldsymbol{\Lambda}} &= \sqrt{\boldsymbol{S}}\boldsymbol{V}^T \end{aligned} \tag{1.42}$$

where, as also seen for SSI-data, the discrete time matrix and observation matrix can be calculated and used for estimation of the MP. [BE15c].

1.2.2.8 Performance

Obtaining accurate estimates of the MP, a suitable model order is required. Several statistical measurements can be used for analysing the performance of the system identification method mentioned in the previous sections. [Ave]. The statistical measurements used throughout this study are:

- RSS/SSS - Residual Sum of Squares over Series Sum of Squares
- BIC - Bayesian Information Criterion
- SPP - Samples Per Parameter
- CN - Condition Number

For the RSS part in RSS/SSS it is simply the sum of the prediction error squared:

$$RSS = \sum_{i=1}^{N} (y_i - \hat{y}_i)^2 \tag{1.43}$$

and to obtain the RSS/SSS the RSS term is then divided by the SSS:

$$SSS = \sum_{i=1}^{N} y_i^2 \tag{1.44}$$

In Equation (1.43) it is obvious that the RSS/SSS should be as low as possible, since the predicted error should be minimized. Likewise for the BIC, which can be calculated as:

$$BIC = N \ln \widehat{\sigma}_w^2 + d \ln N \tag{1.45}$$

Where:

$d =$ the dimension of the parameter vector (number of free parameters)

The measure of BIC should be stabilized in order to have a model that fits the data. [Jam+21].

The CN is the ratio from the largest to lowest eigenvalue of a matrix and is an indicator of the numerical condition of a matrix for inversion. If the CN is high then the numerical sensitivity of the matrix inverse calculation is significant. The importance of the CN is the computational precision. The precision of the calculations in MATLAB is

$$eps = 2.2204 \cdot 10^{-16} \tag{1.46}$$

and if the matrix for inversion is ill-conditioned, it will be sensitive for the computational round-off, which can lead to unstable results. Therefore, the reciprocal of the CN should be more than the precision of the computer. [Roz18].

$$\frac{1}{CN} > eps \tag{1.47}$$

1.3 Uncertainties associated to the modal parameter estimate

Monte Carlo simulations are typically used for estimating an unknown probability function. For simplicity, it is assumed that the MP are normal distributed, since the modelled randomness is normal distributed as well. This is not an exact assumption since non-linearity occurs in the transformation from the state matrix to the MP. With the assumption of normal distribution it is needed to calculate the variance and the mean value. The exact value requires the probability function of the MP to be known, but estimates can be made. The main idea behind the Monte Carlo simulations are to estimate this by conducting a vast series of runs in order to track the randomness. [Joh10]. For each system identification method, stated in Section 1.2.1 and 1.2.2, 100 simulations is estimated to provide acceptable estimates of the variance and the bias and still ease the computational effort to some extent. Increasing the number of simulations should increase the accuracy for the estimated bias and variance, and at some number it should converge to the true value.

1.4 Analytical results

To clarify the analytical MP of the FE model, an overview of the natural frequencies and damping ratios are shown in Table 1.2.

Analytical MP of the FE model				
	Mode 1	Mode 2	Mode 3	Mode 4
Undamped natural frequency [Hz]	71.25	312.38	795.75	1538.62
Damping ratio	0.005	0.01	0.015	0.02

Table 1.2: Analytical MP of the FE model

Results

Before the extracting process of the MP, each method is tuned in order to increase the accuracy. Since the behaviour of each method varies, a general process for all methods does not exists. The main procedure is shown in Figure 2.1. The flow chart describes the process of both the non-parametric method and the parametric method, mentioned in Section 1.2.1 and 1.2.2.

Figure 2.1: Flow chart of the MP extraction and Monte Carlo simulations

2.1 Non-parametric method

First, the process shown in the flow chart, Figure 2.1, is followed for the non-parametric method for estimate the MP of the structure.

2.1.1 Optimizing the accuracy

Following the methodology described in Section 1.2.1.1, the Welch's estimation of the PSD is calculated of the four responses shown in Figure 1.3. By experience and analyzing the estimated PSD the parameters of the Welch's estimation are:

Parameters of Welch's PSD	
Blocksize	$\frac{N}{4}$
Overlap	$\frac{3}{4}$Blocksize
Spectral Window	Hanning

Table 2.1: Parameters used for estimating PSD

The natural frequencies are found as the peak values, and the damping ratios are estimated by 3dB bandwidth, via Equation (1.7). Difficulties arise following this methodology since the PSD from Equation (1.9) consist of frequencies bins which constitute the frequency resolution. If the frequency resolution is not of high quality, the MP can be estimated wrong. Therefore, the PSD is curve fitted before estimating the MP of the fitted curve. The Least-Square Complex Exponential Method is used for fitting the PSD before the MP extraction [MATa].

2.1.2 Estimation of variance and bias

For providing an estimate of the uncertainty bounds associated with the MP, 100 Monte Carlo simulations are conducted, see Section 1.3. Then the estimation of the variance is [MATb]:

$$\widehat{\sigma}^2 = \frac{1}{N-1} \sum_{i=1}^{N} |A_i - \mu|^2 \tag{2.1}$$

and the bias is calculated by subtracting the estimated mean from the actual value:

$$bias = \widehat{\mu} - y \tag{2.2}$$

Then the estimated variance and bias of the first four natural frequencies and the corresponding damping ratios are seen in Figure 2.2

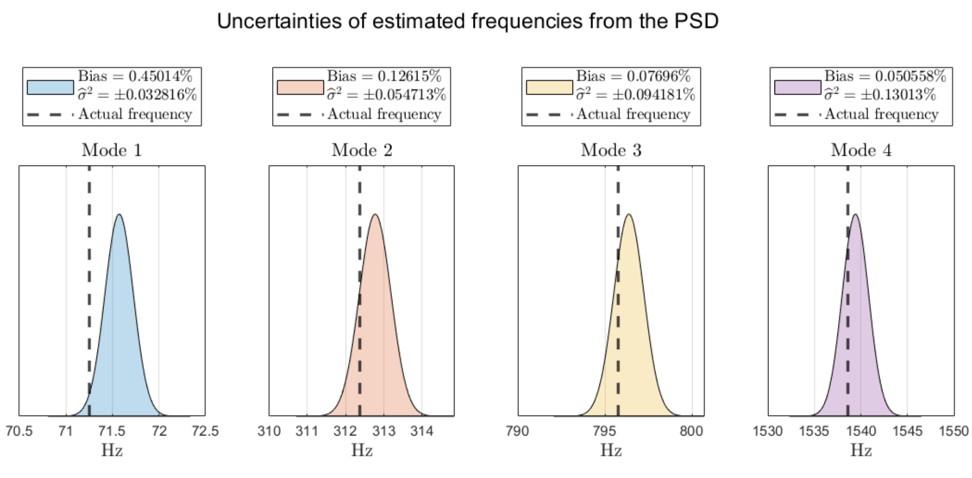

Figure 2.2: Uncertainty bounds of the estimated frequencies extracted from the PSD

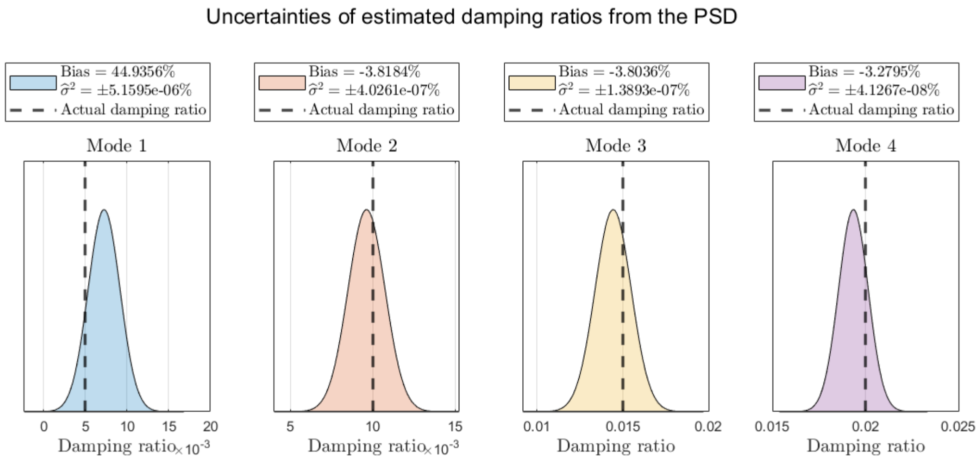

Figure 2.3: Uncertainty bounds of the estimated damping ratios extracted from the PSD

The results from the non-parametric method are gather in Table 2.2.

Estimated variance and bias from the PSD-based method								
PSD-based	Mode 1		Mode 2		Mode 3		Mode 4	
	bias[%]	$\widehat{\sigma}^2$[%]	bias[%]	$\widehat{\sigma}^2$[%]	bias[%]	$\widehat{\sigma}^2$[%]	bias[%]	$\widehat{\sigma}^2$[%]
f_n	0.450	0.033	0.126	0.055	0.077	0.094	0.051	0.130
ζ_n	44.94	5e-6	-3.818	4e-7	-3.804	1e-7	-3.280	4e-8

Table 2.2: Estimated variance and bias associated with the estimated frequencies and damping ratios for non-parametric methods

2.2 Parametric method

Next, the same process shown in the flow chart, Figure 2.1, is followed for the different parametric methods mentioned in Section 1.2.2. The process of increasing the accuracy can be more time-consuming and complicated than for the process in Section 2.1.1.

2.2.1 Optimizing the accuracy

Common for all the proposed methods is the existence of a region where the extracted MP are stable. If the model order of the parametric model is too low, the extracted MP has not become stable yet. But if the model order of the parametric model is too high, the extracted MP starts to be unstable. For selecting this sweet spot area the performance parameters (RSS/SSS, BIC, SPP, CN) in Section 1.2.2.8 are analysed.

For selecting this sweet spot area it is necessary to analyze the frequency stabilization plot up till a too high model order. For the AR models the model is assumed to be too complex if the amount of samples used for estimating the AR-parameters is below 10. The result of this is that the maximum model order can be:

$$n_{max} = \frac{N \cdot n_y \cdot n_x}{n_y \cdot n_y \cdot SPP} \approx 205 \tag{2.3}$$

Where:

$n_y =$ Number of responses
$n_x =$ Number of excitation

The frequency stabilization plot, RSS/SSS, BIC and CN for the VAR model up till a model order of 210 can be seen in Figure 2.4. For the other method mentioned in Section 1.2.2 the frequency stabilization plot can be seen in Appendix A.1

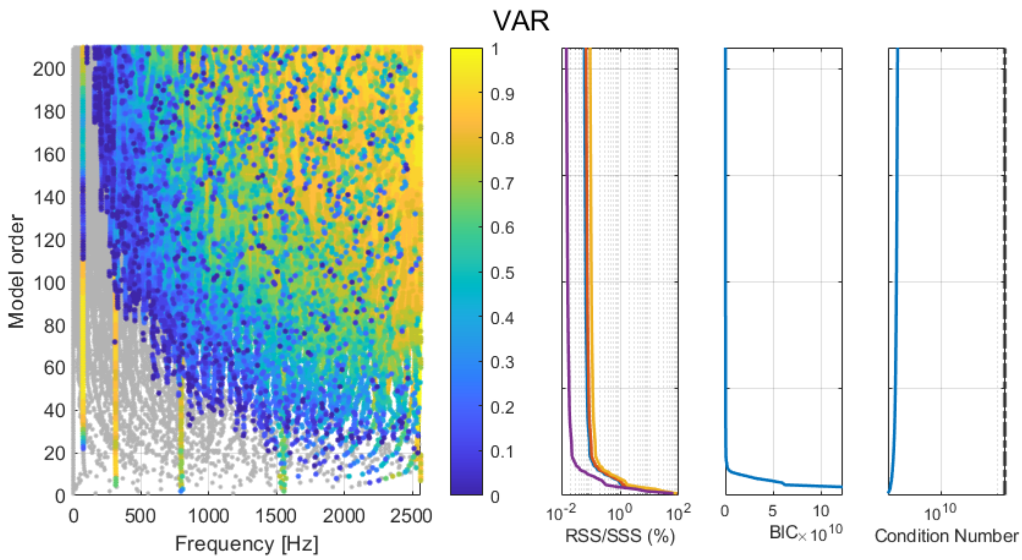

Figure 2.4: Frequency stabilization, RSS/SSS and BIC for VAR-model with a maximum model order of 210

The RSS/SSS and BIC stabilize from a model order of approximately 20. Common for the AR-models is the stability for low order modes. The stability for higher order modes can be difficult to analyze in the frequency stabilization plot, since significant amounts of spurious modes occurs at higher model order. Therefore, the physical modes are extracted to analyze the stability hereof. If the frequency deviates more than 0.5% from the true natural frequency it is labelled as a black cross, Figure 2.5 for the VAR model.

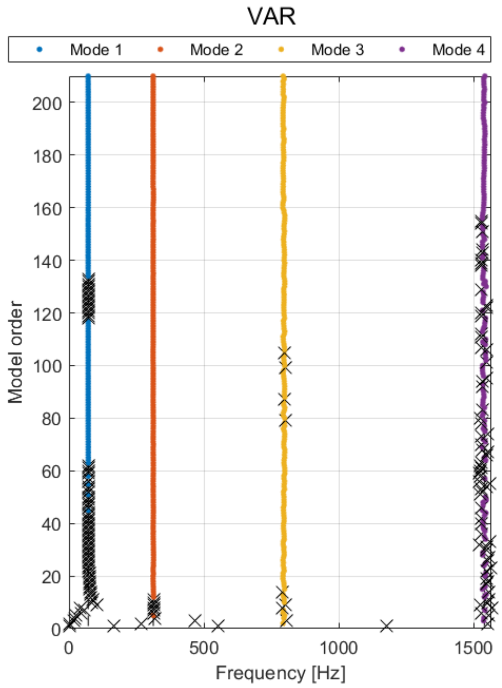

Figure 2.5: Extracted frequencies for the VAR-model for the first 4 modes

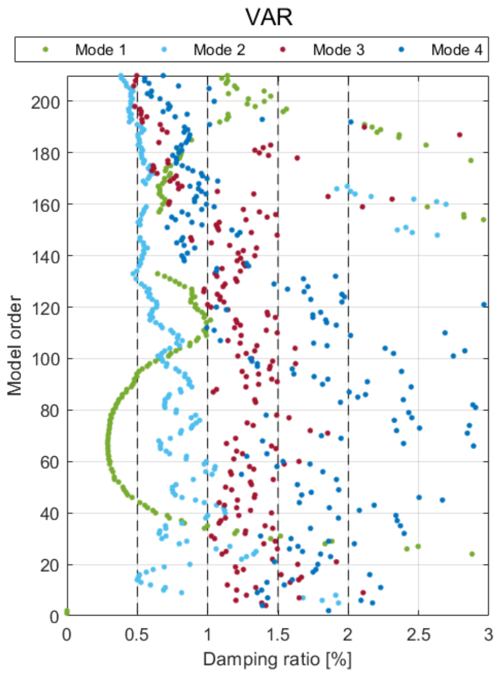

Figure 2.6: Extracted damping ratios for the VAR-model for the first 4 modes

Several stable regions can be seen in Figure 2.5. A suggestive stable region for the VAR model where the first four natural frequencies seems stable is within the span of a model order from 95 to 105. This region is chosen for all the AR models. Similar plots for the other proposed methods are seen in Appendix A.2. The following sweet spot areas are:

Model order of sweet spot area	
MITD OO	75 - 85
MITD IO	75 - 85
ERA OO	70 - 80
ERA IO	70 - 80
SSI OO	70 - 80

Table 2.3: Model order of the sweet spot area

2.2.2 Estimation of variance and bias

The sweet spot areas in Figure 2.5 and Table 2.3 are used through the Monte Carlo simulations to estimate the variance and bias as described in Section 2.1.2. The distributions of the MP estimated from the VAR model are seen in Figure 2.7 and 2.8.

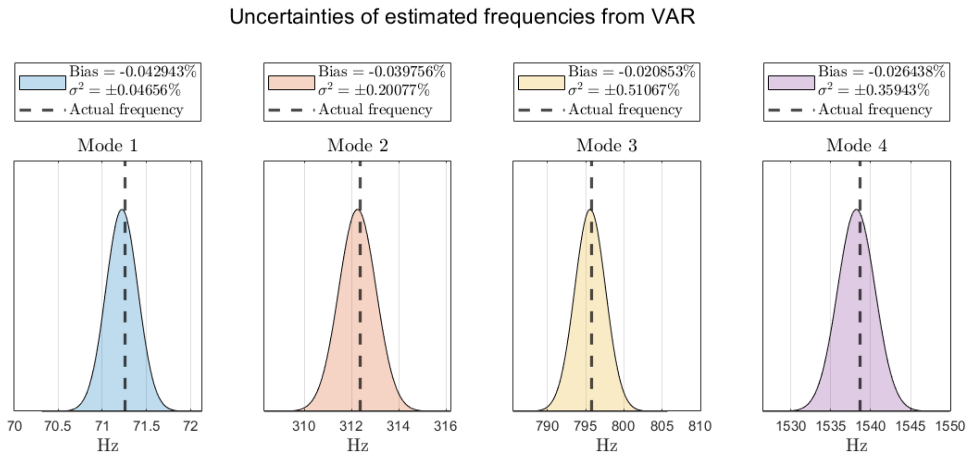

Figure 2.7: Uncertainties of the estimated frequencies extracted from the VAR model

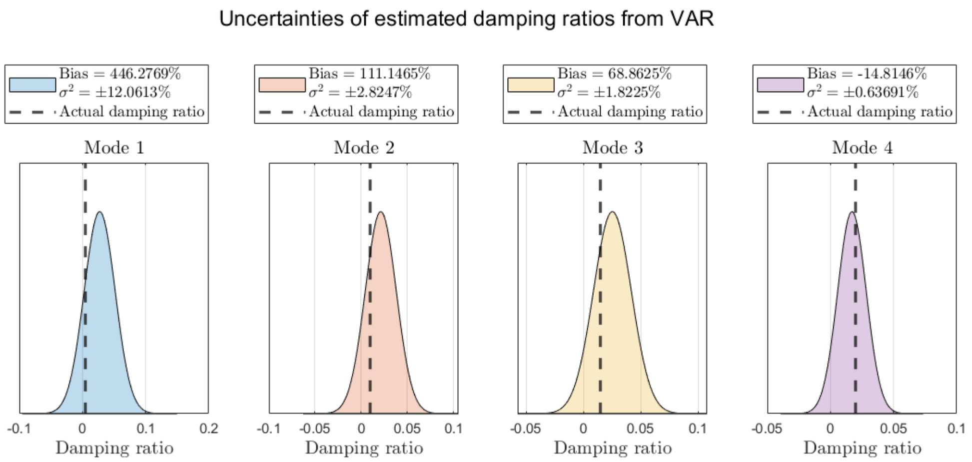

Figure 2.8: Uncertainties of the estimated damping ratios extracted from the VAR model

For all the mentioned parametric methods for system identification, the estimated variance and bias associated with the estimated natural frequencies are shown in Table 2.4. The estimated variance and bias associated with the estimated damping ratios are shown in Table 2.5.

Estimated variance and bias of the estimated frequencies								
Method	Mode 1		Mode 2		Mode 3		Mode 4	
	bias[%]	$\widehat{\sigma}^2$[%]	bias[%]	$\widehat{\sigma}^2$[%]	bias[%]	$\widehat{\sigma}^2$[%]	bias[%]	$\widehat{\sigma}^2$[%]
VAR	-0.043	0.047	-0.040	0.201	-0.021	0.511	-0.026	0.359
VARMA	-0.022	0.064	0.042	0.262	-0.013	0.349	-0.005	0.373
VARX	-0.031	0.024	0.003	0.005	-2e-4	3e-4	-1e-5	6e-7
VARMAX	0.015	0.021	-0.001	0.003	7e-4	2e-3	3e-6	7e-7
MITD-OO	0.362	1.848	0.014	0.163	-0.003	0.247	-0.003	0.337
MITD-IO	0.276	2.773	-0.032	0.047	0.008	0.040	0.016	0.092
ERA-OO	-0.022	0.156	-0.056	0.244	0.055	0.343	0.011	0.453
ERA-IO	0.010	0.036	-0.001	0.007	-0.006	0.030	0.006	0.050
SSI-data	-0.146	0.031	0.013	0.152	0.017	0.558	-0.020	0.617

Table 2.4: Estimated variance and bias associated with the estimated frequencies for parametric methods

Estimated variance and bias of the estimated damping ratios								
Method	Mode 1		Mode 2		Mode 3		Mode 4	
	bias[%]	$\widehat{\sigma}^2$[%]	bias[%]	$\widehat{\sigma}^2$[%]	bias[%]	$\widehat{\sigma}^2$[%]	bias[%]	$\widehat{\sigma}^2$[%]
VAR	446.3	12.06	111.1	2.825	68.86	1.823	-14.81	0.637
VARMA	130.8	5.139	73.70	3.067	19.57	1.867	-36.39	0.479
VARX	127.8	5.517	14.44	0.280	1.159	0.001	-4e-4	8e-7
VARMAX	113.8	4.152	20.36	0.569	0.293	3e-3	-0.057	5e-5
MITD-OO	-1324	143.7	-105.4	3.893	-82.95	0.942	-105.6	0.061
MITD-IO	-2055	84.28	-46.99	8.699	-40.36	4.439	-62.36	4.646
ERA-OO	227.1	12.00	77.85	4.785	-10.84	1.070	-32.32	1.573
ERA-IO	198.0	7.205	37.66	1.849	6.891	0.026	4.277	0.133
SSI-data	337.0	12.65	120.3	3.066	77.86	3.004	-5.444	1.103

Table 2.5: Estimated variance and bias associated with the estimated damping ratios for parametric methods

2.3 Experimental results

For an overview of the experimental results obtain from the Monte Carlo simulations, the mean frequency and the mean damping ratio for the first four modes are calculated and shown with their respective variance from Table 2.2, 2.4 and 2.5 in Figure 2.9 and 2.10 for OO-based system identification and in Figure 2.11 and 2.12 for IO-based system identification

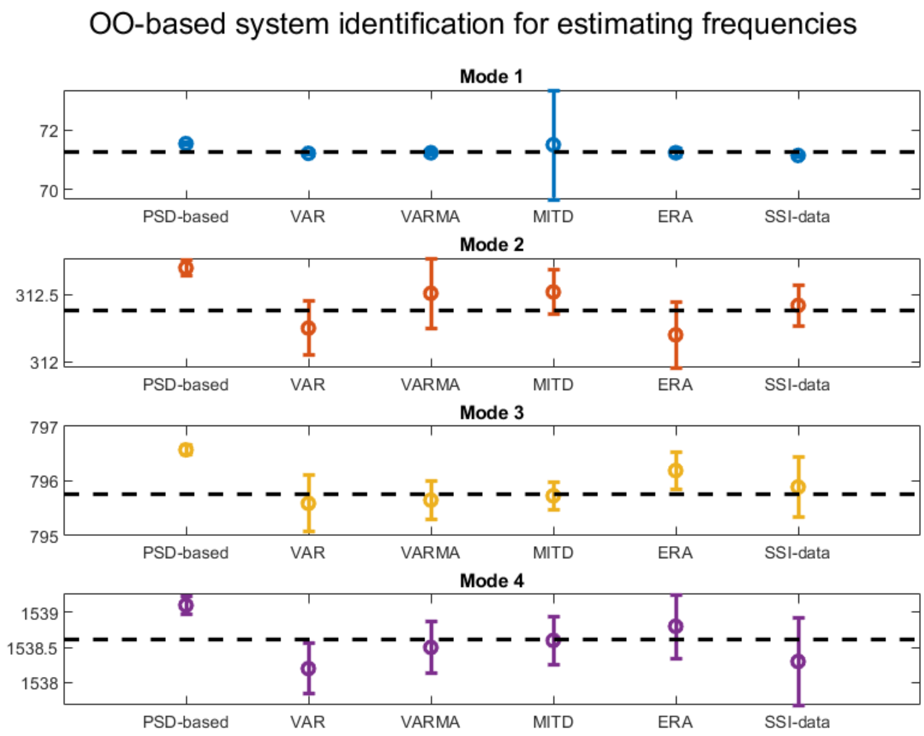

Figure 2.9: Mean of the estimated frequencies and their variance for the OO-based system identification. The black dashed line represent the exact value.

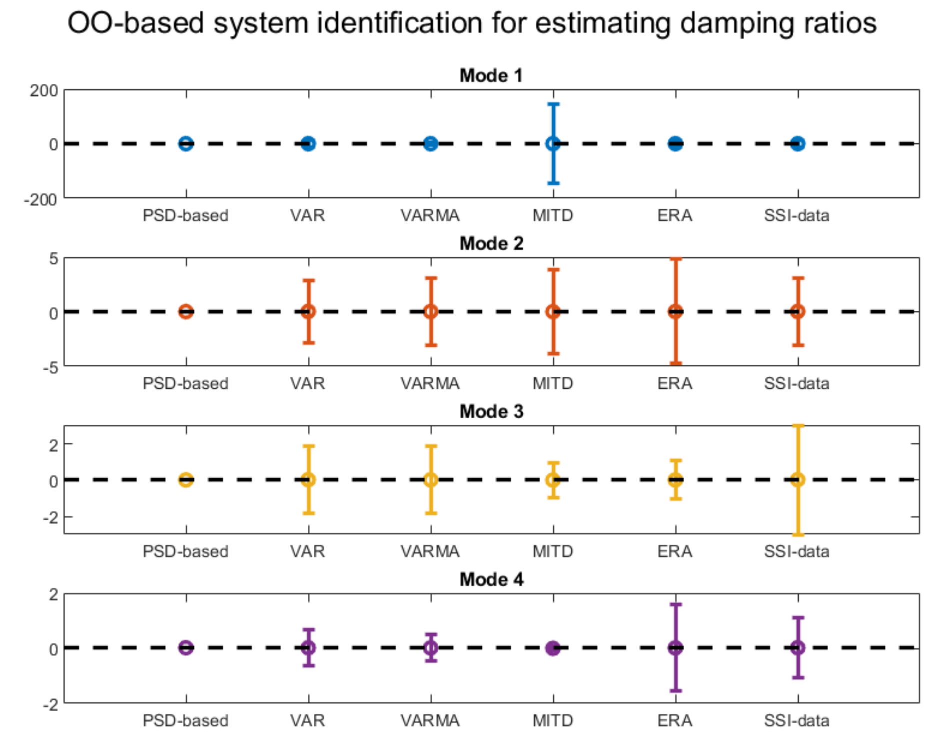

Figure 2.10: Mean of the estimated damping ratios and their variance for the OO-based system identification. The black dashed line represent the exact value.

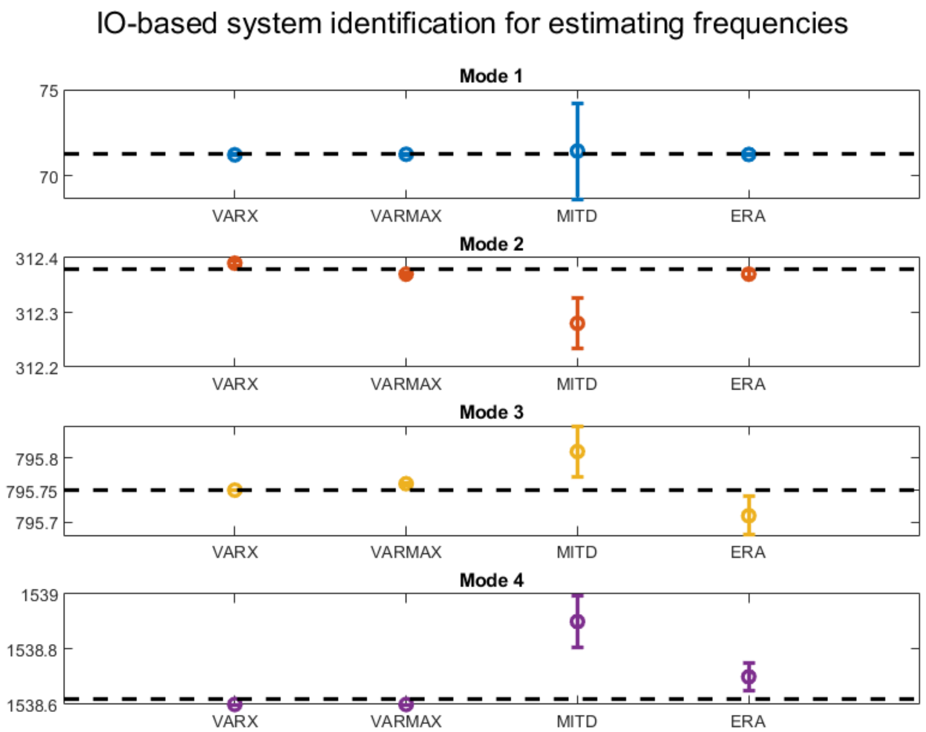

Figure 2.11: Mean of the estimated frequencies and their variance for the IO-based system identification. The black dashed line represent the exact value.

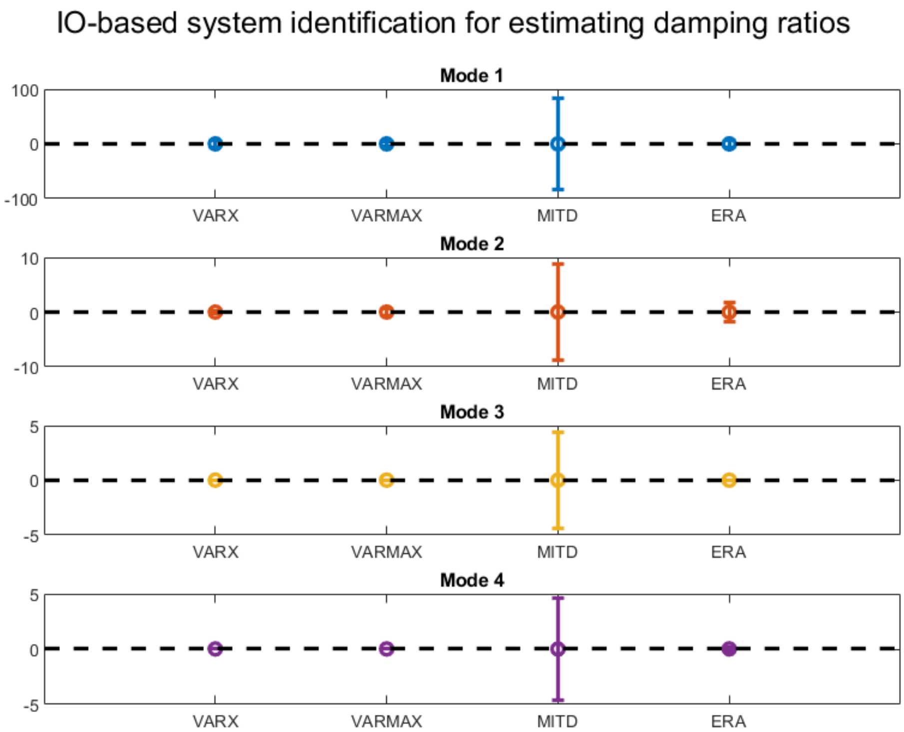

Figure 2.12: Mean of the estimated damping ratios and their variance for the IO-based system identification. The black dashed line represent the exact value.

Interpretation of results

An interpretation of the results presented in Figure 2.9, 2.10, 2.11 and 2.12 is necessary before concluding which method that might have the best performance for the given structure. It is not straight forward to compare all the used methods for MP extraction, since the basis of them are not the same. Theoretically, the accuracy is increased significantly if the system identification is IO-based. This is due to the fact that the dynamics of the excitation do not impact the estimation of the MP in the same way if the system identification were OO-based [Bra11]. Therefore, it is more convenient to perform a comparative analysis of the IO-based and of the OO-based instead of a single comparison.

3.1 OO-based system identification

OO-based system identification does not have the advantage of knowing the dynamics of the excitation. Therefore, the estimated MP can be contaminated to some extent. The OO-based system identification methods used for MP extraction are the PSD-based, the VAR, the VARMA, the MITD, the ERA, and the SSI-data, see Figure 2.9 and 2.10 and Table 2.4 and 2.5.

Common for all of them are the poor estimation of the damping ratios. Even though the damping ratio associated with the first mode have a bias 45%, the PSD-based method performs acceptable for estimating the damping ratios compared to the other OO-based methods. It is worth mentioning that for extracting the MP from the PSD, a parametric representation were made using The Least-Square Complex Exponential Method, as mentioned in Section 2.1.1. With the doubtfulness of being a non-parametric or parametric method, the use of the PSD-based method for MP extraction still have a higher simplicity. Furthermore, accuracy of the estimated MP from the PSD-based method might drop if the signal is more contaminated with noise.

When estimating the natural frequencies higher accuracy in terms of less bias can be seen for the parametric methods. An overall analysis of the first four estimated frequencies, the VAR and the VARMA models have a slight higher accuracy in terms of less bias but almost similar to the SSI-data. For the second, third and fourth mode the AR models are outperformed by the MITD when analyzing the bias of the estimated frequencies. But analyzing the variance associated with the estimated frequencies comes with another statement. Overall, the VAR model has smaller variance than the VARMA model. Furthermore, the SSI-data has the less variance for the first two modes, where it is then outperformed by the MITD for the third and fourth mode when it comes to having less variance.

3.2 IO-based system identification

The use of IO-based system identification method requires the excitation to be measured. This is to some extent only possible for EMA, since several EOV can be present in the excitation in real life, making IO-based system identification near impossible for OMA. The IO-based system identification methods used for MP extraction are the VARX, the VARMAX, the MITD and the ERA, see Figure 2.11 and 2.12 and Table 2.4 and 2.5.

The estimation of the damping ratios improves significantly for IO-based system identifications, seen in Table 2.5, especially for the VARX and VARMAX model. But all of them have a poor estimation of the damping ratio of the first mode. This might be due to damping being the 3dB bandwidth of the resonance and the power associated with low power modes can be sensitive to noise. Discarding the poor estimation of the damping ratios for the first two modes, the VARMAX has a superior accuracy of estimating the damping ratios. The MITD is seen to have the worst performance of estimating the damping ratios, see Figure 2.12.

Higher accuracy for estimating the frequencies can also be seen for most of the IO-based system identification methods. Both the VARX and VARMAX models has a high accuracy bound to the estimation of the first four frequencies. The IO-based MITD and ERA has a slight improvement compared to their OO-based versions, but still being outperformed by the VARX and VARMAX models.

Conclusion

Several system identification methods, where the main concept has been briefly introduced, for extraction of the MP have been tested. The system identification methods used throughout the study are the *Power Spectral Density* (PSD), the *AutoRegressive* (AR) models (namely the VAR, VARMA, VARX and VARMAX), the *Modified Ibrahim Time-Domain* (MITD), the *Stochastic Subspace Identification* (SSI), and the *Eigensystem Realization Algorithm* (ERA). By the use of the Monte Carlo simulations, which were found by state-of-the-art investigations to deliver valid uncertainty bounds of the MP, a comparative analysis of the different system identification methods was done. Since two main categories for the basis of the system identification methods were present, the comparative analysis was divided into two. Therefore, a conclusion on both categories should be conducted.

In the context of OMA the excitation is not measured typically. Furthermore, since the main excitation source is the wind which is low-frequency excitation, higher-order modes are not excited necessarily. Therefore, it is wanted to have high accuracy for low order modes. To predict damages as early as possible, the variance bound to the estimated frequencies should be minimized. With this in mind, the PSD-based method, the VAR model, and the VARMA model performed well for the given structure.

If the excitation is measured, which is considered as being EMA, both the bias and the variance of the estimated MP are reduced significantly, especially for *Input-Output* (IO) based VAR and VARMA models (VARX and VARMAX). For the first two modes the IO-based ERA has similar accuracy, but with higher levels of variance than the VARX and VARMAX models. One major disadvantage of the IO-based system identification methods is the requirement of the excitation is measured. Therefore, in the context of a SHM-system, it would not make sense to aim the study on IO-based system identification methods.

The overall conclusion from this study and in the context of a SHM-system is not aimed at a single system identification method that outperforms the other methods. The PSD-based method, the VAR model, and the VARMA model showed high accuracy for the FE representation of a laboratory-scaled wind turbine blade. Therefore, these three methods are recommended for further study of the real laboratory-scaled wind turbine blade to investigate the uncertainty bounds hereof. If the process is solely related to damage detection, then the VARX and VARMAX models are recommended for further study.

Bibliography

[AC19] Luis David Avendaño-Valencia and Eleni N. Chatzi. “Modelling long-term vibration monitoring data with Gaussian Process time-series models”. In: *IFAC-PapersOnLine* 52.28 (2019), pp. 26–31. ISSN: 24058963. DOI: 10.1016/j.ifacol.2019.12.343. URL: https://linkinghub.elsevier.com/retrieve/pii/S2405896319322438 (visited on 05/05/2022).

[Ave] Luis David Avendaño-Valencia. *Parametric time-series methods for identification of LTI systems*. (Visited on 05/18/2022).

[BE15a] Rune Brincker and Carlos E. Ventura. “Chapter 2 - Random Variables and Signals”. In: *Introduction to Operational Modal Analysis*. Wiley, 2015, pp. 17–32. ISBN: 978-1-119-96315-8. (Visited on 03/19/2022).

[BE15b] Rune Brincker and Carlos E. Ventura. “Chapter 6 - Random Vibrations”. In: *Introduction to operation modal analysis*. Wiley, 2015, pp. 123–147. ISBN: 978-1-119-96315-8. (Visited on 03/18/2022).

[BE15c] Rune Brincker and Carlos E. Ventura. “Chapter 9 - Time Domain Identification”. In: *Introduction to Operational Modal Analysis*. Wiley, 2015, pp. 239–258. ISBN: 978-1-119-96315-8. (Visited on 05/20/2022).

[Bra11] Anders Brandt. *Noise and vibration analysis: signal analysis and experimental procedures*. OCLC: ocn664324149. Chichester: Wiley, 2011. 438 pp. ISBN: 978-0-470-74644-8.

[BV15] Rune Brincker and Carlos Ventura. *Introduction to operational modal analysis*. Chichester, West Sussex: John Wiley and Sons, Inc, 2015. 1 p. ISBN: 978-1-118-53515-8 978-1-118-53516-5.

[Cha+21] Kartik Chandrasekhar et al. “Damage detection in operational wind turbine blades using a new approach based on machine learning”. In: *Renewable Energy* 168 (May 2021), pp. 1249–1264. ISSN: 09601481. DOI: 10.1016/j.renene.2020.12.119. URL: https://linkinghub.elsevier.com/retrieve/pii/S0960148120320590 (visited on 05/05/2022).

[GF16] A. Gómez González and S.D. Fassois. "A supervised vibration-based statistical methodology for damage detection under varying environmental conditions & its laboratory assessment with a scale wind turbine blade". In: *Journal of Sound and Vibration* 366 (Mar. 2016), pp. 484–500. ISSN: 0022460X. DOI: 10.1016/j.jsv.2015.11.018. URL: https://linkinghub.elsevier.com/retrieve/pii/S0022460X15009153 (visited on 05/25/2022).

[Gre+22] Szymon Greś et al. "Uncertainty quantification of modal parameter estimates obtained from subspace identification: An experimental validation on a laboratory test of a large-scale wind turbine blade". In: *Engineering Structures* 256 (Apr. 2022), p. 114001. ISSN: 01410296. DOI: 10.1016/j.engstruct.2022.114001. URL: https://linkinghub.elsevier.com/retrieve/pii/S0141029622001511 (visited on 04/22/2022).

[Has15] Philipp Ulrich Haselbach. *Ultimate Strength of Wind Turbine Blades under Multiaxial Loading*. PhD Thesis. Orbit DTU: DTU, 2015, p. 62. URL: https://orbit.dtu.dk/en/publications/ultimate-strength-of-wind-turbine-blades-under-multiaxial-loading (visited on 03/17/2022).

[Jam+21] Gareth James et al. *An introduction to statistical learning: with applications in R*. Second edition. Springer texts in statistics. New York: Springer, 2021. 607 pp. ISBN: 978-1-07-161417-4.

[Joh10] A.M. Johansen. "Monte Carlo Methods". In: *International Encyclopedia of Education*. Elsevier, 2010, pp. 296–303. ISBN: 978-0-08-044894-7. DOI: 10.1016/B978-0-08-044894-7.01543-8. URL: https://linkinghub.elsevier.com/retrieve/pii/B9780080448947015438 (visited on 05/23/2022).

[MATa] MATLAB. *modalfit*. https://se.mathworks.com. URL: https://se.mathworks.com/help/signal/ref/modalfit.html?searchHighlight=modalfit&s_tid=srchtitle_modalfit_1 (visited on 03/25/2022).

[MATb] MATLAB. *var*. se.mathworks.com. URL: https://se.mathworks.com/help/matlab/ref/var.html (visited on 05/31/2022).

[Mei] Suzi Mein. *Wind Farm Maintenance Planning*. URL: https://www.firetrace.com/fire-protection-blog/wind-farm-maintenance (visited on 04/24/2022).

[Per+20] Sérgio Pereira et al. "The role of modal parameters uncertainty estimation in automated modal identification, modal tracking and data normalization". In: *Engineering Structures* 224 (Dec. 2020), p. 111208. ISSN: 01410296. DOI: 10.1016/j.engstruct.2020.111208. URL: https://linkinghub.elsevier.com/retrieve/pii/S0141029620338098 (visited on 05/10/2022).

[PP22] Josué Pacheco-Chérrez and Oliver Probst. "Vibration-based damage detection in a wind turbine blade through operational modal analysis under wind excitation". In: *Materials Today: Proceedings* 56 (2022), pp. 291–297. ISSN: 22147853. DOI: 10.1016/j.matpr.2022.01.159. URL: https://linkinghub.elsevier.com/retrieve/pii/S2214785322001869 (visited on 04/21/2022).

[Roz18] Michael Rozman. *What is the condition number of a matrix?* Mar. 7, 2018. URL: https://www.phys.uconn.edu/~rozman/Courses/m3511_18s/downloads/condnumber.pdf (visited on 04/30/2022).

[RPD08] Edwin Reynders, Rik Pintelon, and Guido De Roeck. "Uncertainty bounds on modal parameters obtained from stochastic subspace identification". In: *Mechanical Systems and Signal Processing* 22.4 (May 2008), pp. 948–969. ISSN: 08883270. DOI: 10.1016/j.ymssp.2007.10.009. URL: https://linkinghub.elsevier.com/retrieve/pii/S0888327007002257 (visited on 05/18/2022).

[TD14] Gilles Tondreau and Arnaud Deraemaeker. "Numerical and experimental analysis of uncertainty on modal parameters estimated with the stochastic subspace method". In: *Journal of Sound and Vibration* 333.18 (Sept. 2014), pp. 4376–4401. ISSN: 0022460X. DOI: 10.1016/j.jsv.2014.04.039. URL: https://linkinghub.elsevier.com/retrieve/pii/S0022460X14003253 (visited on 05/20/2022).

Frequency stabilization

A.1 Frequency stabilization plot and performance parameters

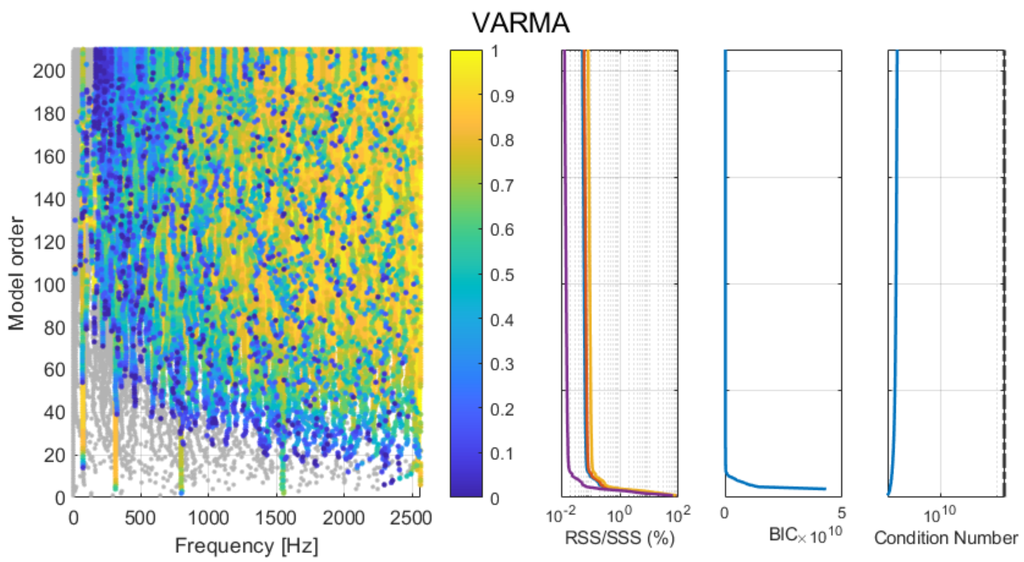

Figure A.1: Frequency stabilization, RSS/SSS and BIC for VARMA-model with a maximum model order of 210

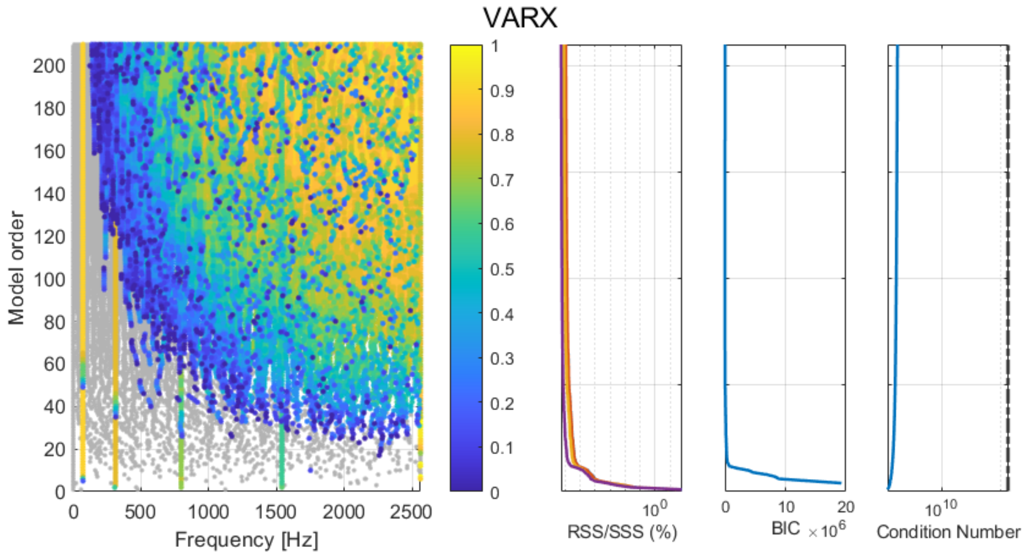

Figure A.2: Frequency stabilization, RSS/SSS and BIC for VARX-model with a maximum model order of 210

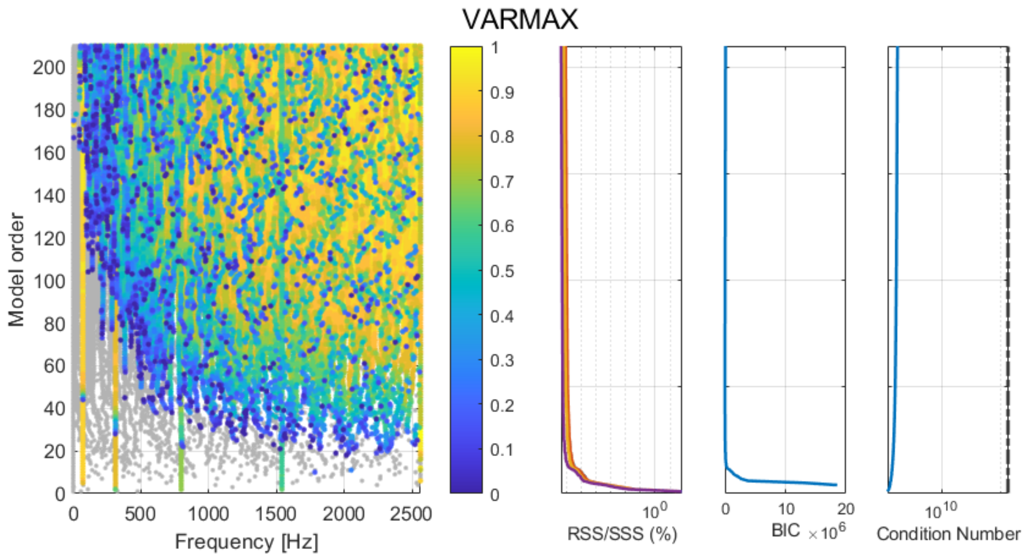

Figure A.3: Frequency stabilization, RSS/SSS and BIC for VARMAX-model with a maximum model order of 210

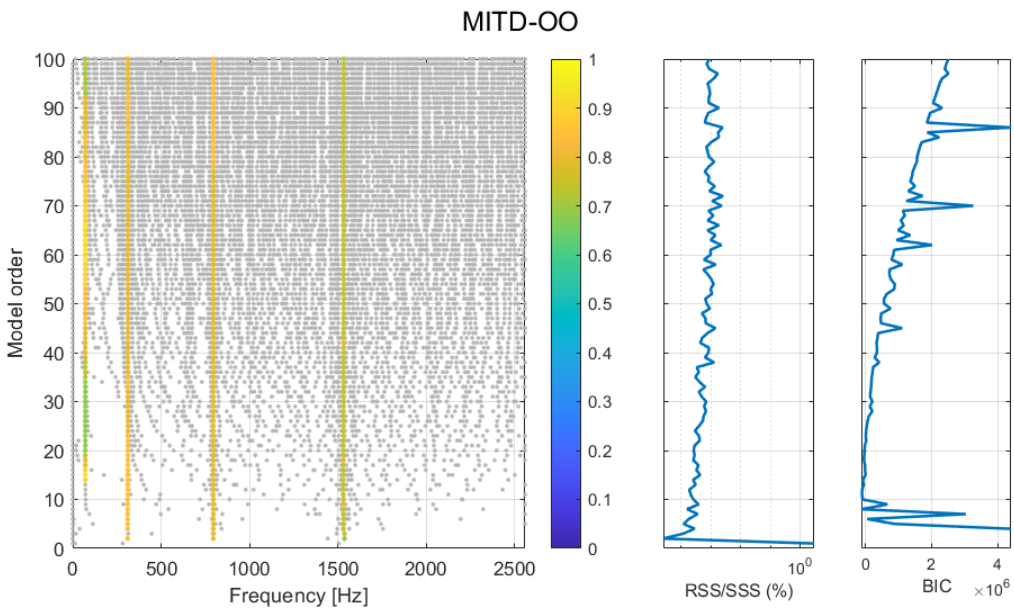

Figure A.4: Frequency stabilization, RSS/SSS and BIC for MITD model Output Only with a maximum model order of 100

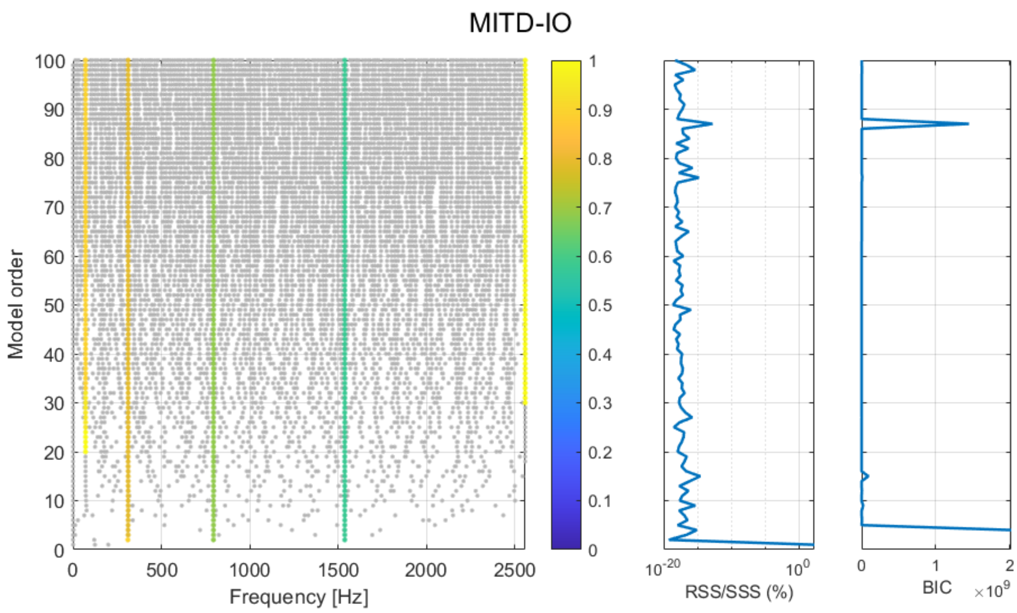

Figure A.5: Frequency stabilization, RSS/SSS and BIC for MITD model Input Output with a maximum model order of 100

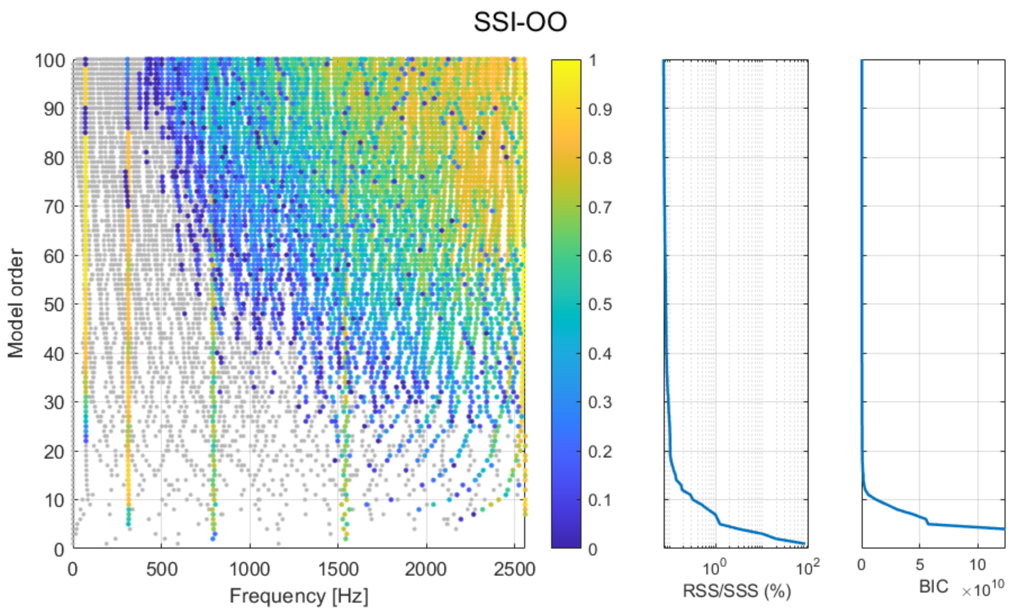

Figure A.6: Frequency stabilization, RSS/SSS and BIC for SSI model Output Only with a maximum model order of 100

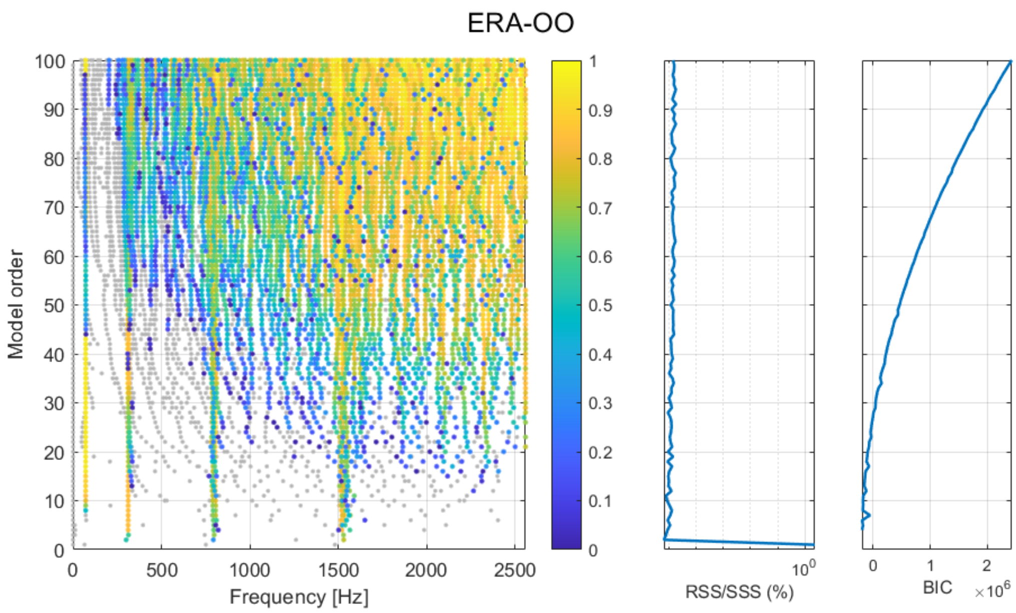

Figure A.7: Frequency stabilization, RSS/SSS and BIC for ERA model Output Only with a maximum model order of 100

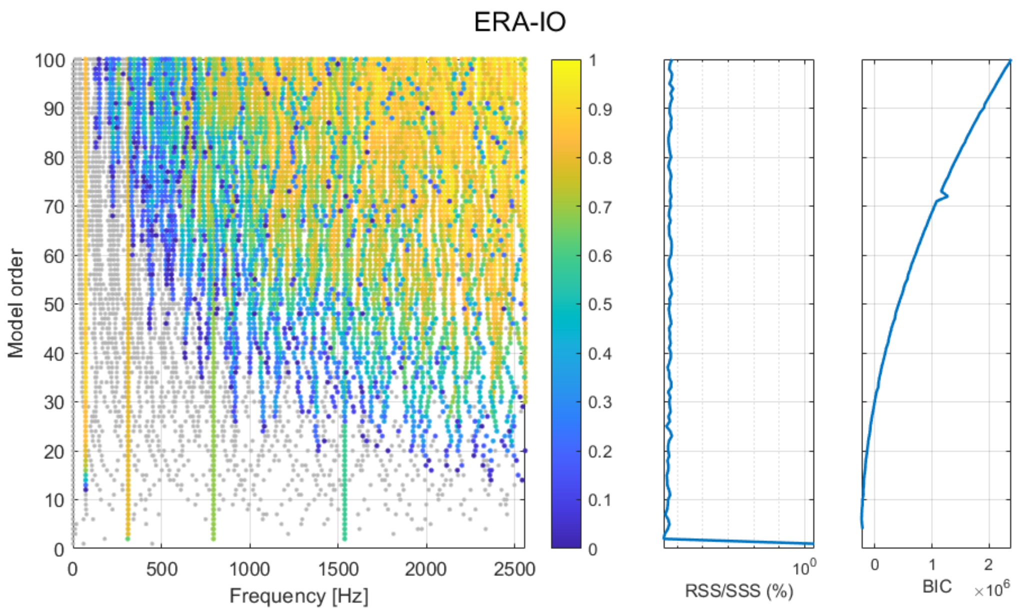

Figure A.8: Frequency stabilization, RSS/SSS and BIC for ERA model Input Output with a maximum model order of 100

A.2 Stabilization of first four frequencies

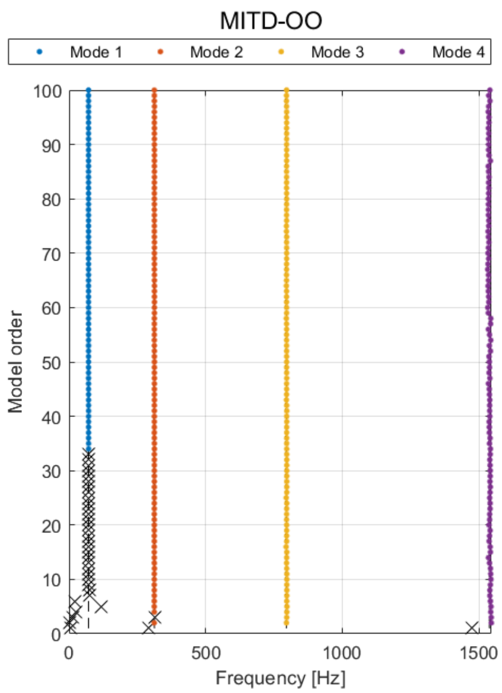

Figure A.9: Extracted frequencies for the MITD OO model for the first 4 modes

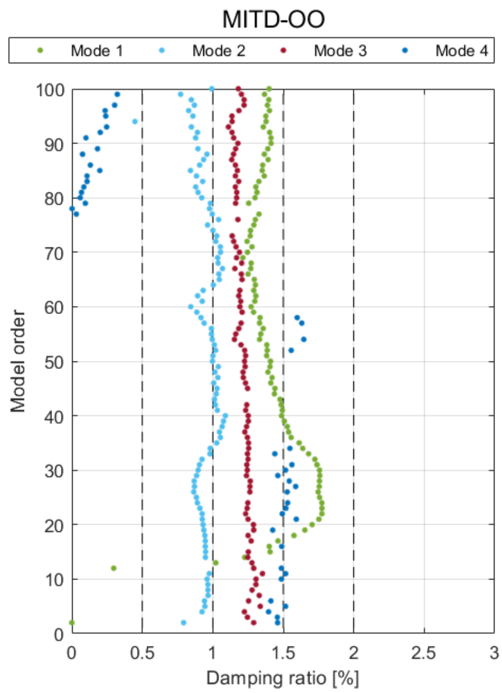

Figure A.10: Extracted damping ratios for the MITD OO model for the first 4 modes

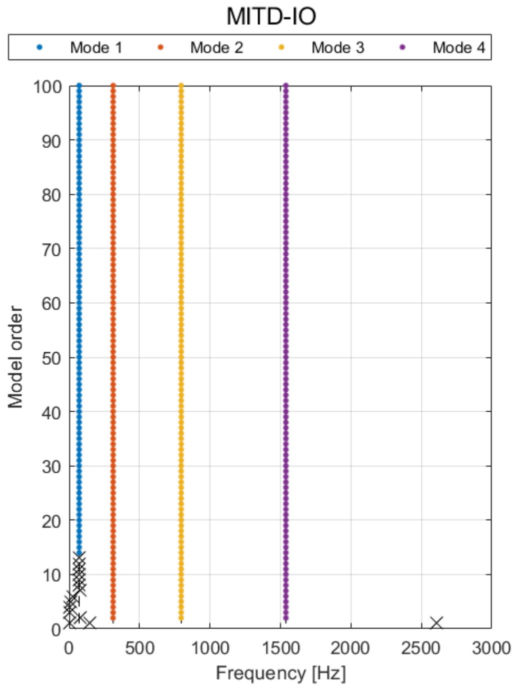

Figure A.11: Extracted frequencies for the MITD IO model for the first 4 modes

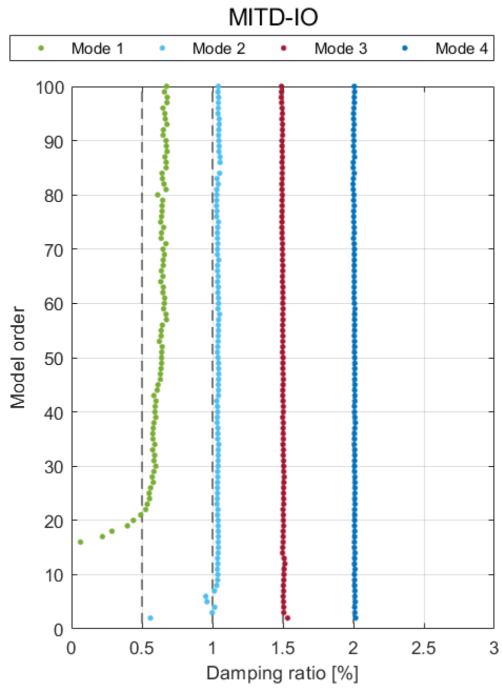

Figure A.12: Extracted damping ratios for the MITD IO model for the first 4 modes

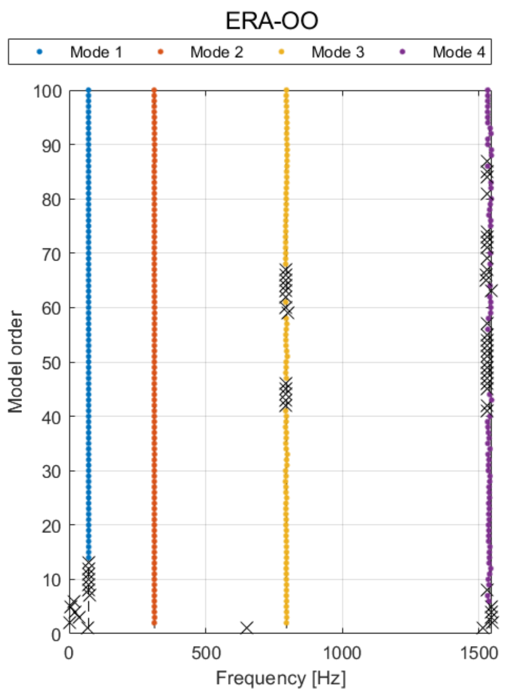

Figure A.13: Extracted frequencies for the ERA OO model for the first 4 modes

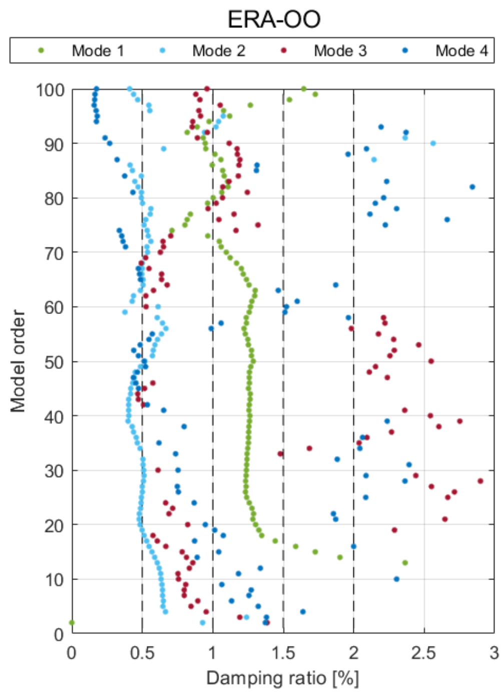

Figure A.14: Extracted damping ratios for the ERA OO model for the first 4 modes

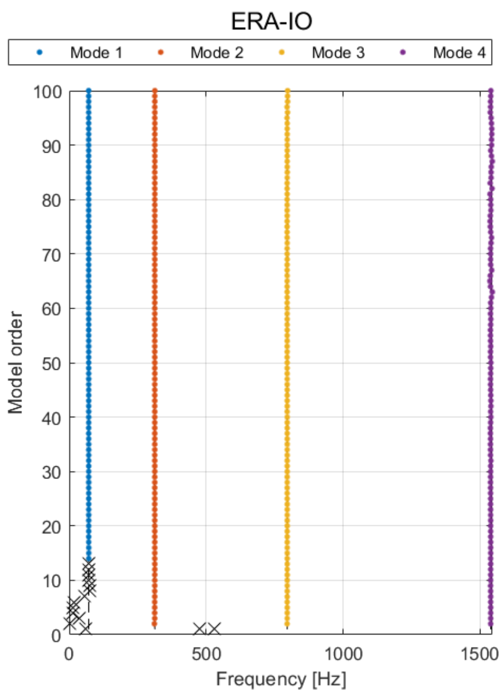

Figure A.15: Extracted frequencies for the ERA IO model for the first 4 modes

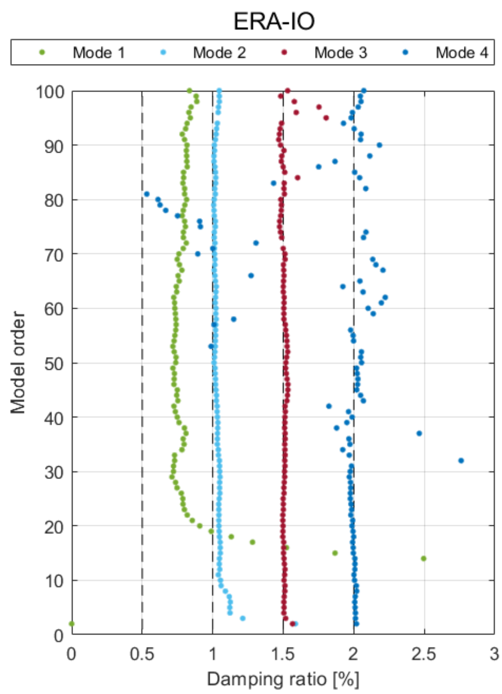

Figure A.16: Extracted damping ratios for the ERA IO model for the first 4 modes

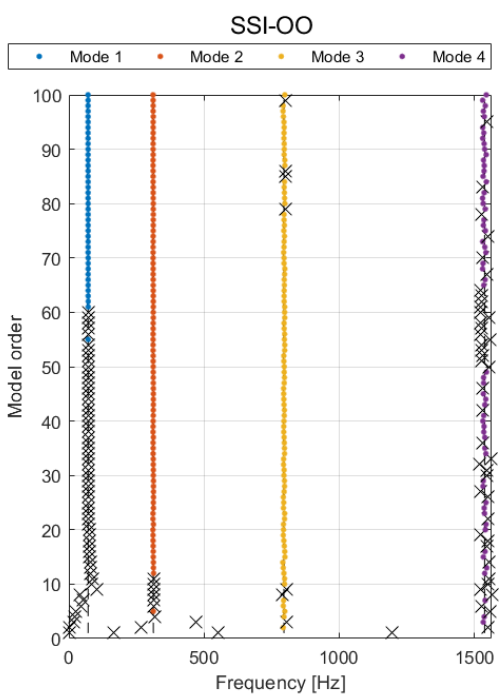

Figure A.17: Extracted frequencies for the SSI OO model for the first 4 modes

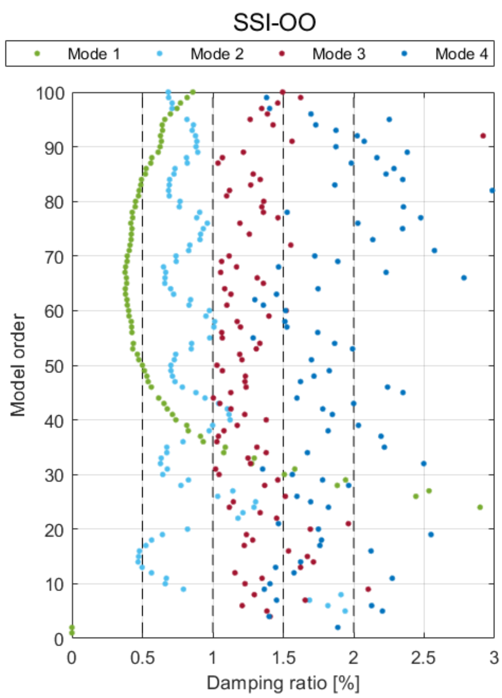

Figure A.18: Extracted damping ratios for the SSI OO model for the first 4 modes